

# Forced linear shear flows with rotation: rotating Couette-Poiseuille flow, its stability and astrophysical implications

SUBHAM GHOSH<sup>1</sup> AND BANIBRATA MUKHOPADHYAY<sup>1</sup>

<sup>1</sup> *Department of Physics, Indian Institute of Science, Bangalore 560012, India\**

## ABSTRACT

We explore the effect of forcing on the linear shear flow or plane Couette flow, which is also the background flow in the very small region of the Keplerian accretion disk. We show that depending on the strength of forcing and boundary conditions suitable for the systems under consideration, the background plane shear flow and, hence, accretion disk velocity profile modifies to parabolic flow, which is plane Poiseuille flow or Couette-Poiseuille flow, depending on the frame of reference. In the presence of rotation, plane Poiseuille flow becomes unstable at a smaller Reynolds number under pure vertical as well as three-dimensional perturbations. Hence, while rotation stabilizes plane Couette flow, the same destabilizes plane Poiseuille flow faster and forced local accretion disk. Depending on the various factors, when local linear shear flow becomes Poiseuille flow in the shearing box due to the presence of extra force, the flow becomes unstable even for the Keplerian rotation and hence turbulence will pop in there. This helps in resolving a long standing problem of sub-critical transition to turbulence in hydrodynamic accretion disks and laboratory plane Couette flow.

*Keywords:* Accretion – Hydrodynamics – Compact objects – Astrophysical fluid dynamics

## 1. INTRODUCTION

Accretion disks are very exotic astrophysical objects. They are formed around a denser and heavier object, mainly in the form of disk due to the accretion of matter from surroundings. We are particularly interested in the region where the gravitational force almost balances the centrifugal force. This region is called the Keplerian region, and the flow therein is called the Keplerian flow. This flow is stable under linear perturbation, and this stability is called Rayleigh stability.

Nevertheless, to explain the observed physical quantities such as temperature, luminosity, etc. based on the Keplerian disks (see, e.g., Frank et al. 2002), the flow therein must be assumed turbulent. Otherwise, there will be a mismatch of physical quantities, e.g. temperature, of the orders of magnitude between theory and observations. Shakura & Sunyaev (1973) and Lynden-Bell & Pringle (1974) then came up with the idea of turbulent viscosity which is responsible for the transport of matter inward in accretion disks and hence the physical observables. However, the reason behind the turbulence was not known until Balbus & Hawley (1991) proposed an idea of instability involving the coupling between the rotation of fluid and the weak magnetic field therein

following Velikhov (1959) and Chandrasekhar (1960). This instability is known as magneto-rotational instability (MRI), which could bring nonlinearity into the system and hence turbulence. Later, Ogilvie & Pringle (1996) investigated MRI based on a more complicated analysis. Although, MRI succeeds greatly in explaining the origin of turbulence in most of the hot flows, it fails to explain the same in several sites, e.g. protoplanetary disk (Bai 2017, 2013), cataclysmic variables in their low states (Gammie & Menou 1998; Menou 2000), the outer part of active galactic nucleus (AGN) disks and the underlying dead zone (Menou & Quataert 2001). MRI gets suppressed in these cases due to very small ionization of the matter therein. Apart from these, the systems with huge Reynolds number ( $\gtrsim 10^9$ ), as argued by Nath & Mukhopadhyay (2015), have larger growth rate due to magnetic transient growth than the growth rate due to MRI. Bhatia & Mukhopadhyay (2016) however showed that even transient energy growth is ceased to occur beyond a certain magnetic field in magnetohydrodynamical shear flows. Pessah & Psaltis (2005) and Das et al. (2018), using local and global analysis respectively, showed the stabilization of the axisymmetric MRI above a certain magnitude of a toroidal component of the magnetic field for compressible and differentially rotating flows. All these publications showed that MRI is not a generic way to make the Keplerian flow unstable

\* subham@iisc.ac.in (SG), bm@iisc.ac.in (BM)

and hence turbulent. As hydrodynamics is generically there, it is worth looking for plausible hydrodynamic instability instead.

However, the Keplerian flow is Rayleigh stable and there is a long debate in the literature (Dubrulle et al. 2005a,b; Dauchot & Daviaud 1995; Rüdiger & Zhang 2001; Klahr & Bodenheimer 2003; Richard & Zahn 1999; Kim & Ostriker 2000; Mahajan & Krishan 2008; Yecko 2004; Mukhopadhyay et al. 2011; Mukhopadhyay & Chattopadhyay 2013) regarding the stability of Rayleigh stable flows, especially in the context of accretion disks. The authors put forward their efforts to resolve this issue either analytically or with simulation or experimentally. The authors like Balbus et al. (1996) and Hawley et al. (1999) concluded that the sustained turbulence was not possible in the Keplerian flow from hydrodynamics. Nevertheless, other authors, such as Lesur & Longaretti (2005) strongly disagreed with it and discussed about the unavailability of the computer resources to resolve the Keplerian regime. However, with their extrapolated numerical data, they could not produce astrophysically sufficient subcritical turbulent transport in the Keplerian flow. There are other authors too who argued for plausible emergence of hydrodynamical instability and hence further turbulence, by transient growth in the case of otherwise linearly stable flows (e.g. Chagelishvili et al. 2003; Tevzadze et al. 2003; Mukhopadhyay et al. 2011, 2005; Afshordi et al. 2005; Cantwell et al. 2010), in laboratory experiment (e.g. Paoletti et al. 2012), in simulations in case of accretion disks (e.g. Avila 2012).

We, therefore, look for hydrodynamics that could plausibly give rise to unstable modes when the dynamics of the fluid parcel is studied in a small cubical shearing box (see, e.g., Mukhopadhyay et al. 2005; Ghosh & Mukhopadhyay 2020, for details) situated at a particular radius in the Keplerian disk. We are particularly motivated and inspired by our recent results (Ghosh & Mukhopadhyay 2020), which explored in detail the effect of forcing in the linearly and nonlinearly perturbed plane shear flows, with and without rotation, which enlightened the issue of the origin of hydrodynamical turbulence. In fact, there are other works (Ioannou & Kakouris 2001; Mukhopadhyay & Chattopadhyay 2013; Nath & Mukhopadhyay 2016; Razdoburdin 2020) considered an extra forcing to be present in the system. However, in the shearing box, the background flow is of linear shear profile up to first order approximation (see Appendix A and Balbus et al. 1996, for details). This linear shear flow is called plane Couette flow. As in the accretion disk, the shearing box is situated at a particular radius, it will have an angular frequency. We,

therefore, have to consider the effect of rotation while we describe the motion of the accretion disk fluid parcel inside the shearing box. Now, if an extra force is present there in the shearing box, the background flow no longer remains to be linear shear, instead becomes quadratic shear flow what we call plane Couette-Poiseuille flow generally. However, with proper transformation, this flow can be transformed into plane Poiseuille flow. This flow further will embed with rotation in the context of Keplerian flow. Plane Poiseuille flow without rotation is unstable under linear twodimensional perturbation having critical Reynolds number 5772.22 with critical wave vector 1.02 (Orszag 1971). Once it is established that the very local flow (inside the box) in the Keplerian region with forcing is plane Poiseuille flow with rotation, then we can argue that the flow inside the shearing box is unstable. We therefore plan to explore plane Poiseuille flow in the presence of rotational effect. Although, the effect of rotation on the stability of Poiseuille flow was studied by Lezius & Johnston 1976; Alfredsson & Persson 1989, our work is different from them in two aspects. First, we extensively study the eigenspectra of plane Poiseuille flow, as well as Couette-Poiseuille flow, with rotation for purely vertical perturbations and three-dimensional perturbations. To the best of our knowledge, this study has not been done in an extensive manner yet, particularly the effect of rotation on the stability analysis of Couette-Poiseuille flow. Although the Poiseuille flow in the presence of rotation has been studied earlier, to our knowledge, its application to the stability of accretion flow has never been explored. Apart from that, analysis of eigenspectra for Poiseuille flow in the presence of rotation has not been performed yet extensively. However see, e.g., Hains 1967; Cowley & Smith 1985; Balakumar 1997; Savenkov 2010; Klotz et al. 2017, for various explorations of Couette-Poiseuille flow over the years. Second, the background flow profile that we consider here is different than those already considered in previous works (see Lezius & Johnston 1976; Alfredsson & Persson 1989, for details).

The plan of the paper is the following. In §2, we show how the linear shear flow (or plane Couette flow) modifies due to the presence of extra force in the system. In a recent work, we assumed that background does not practically change due to forcing (Ghosh & Mukhopadhyay 2020), here however we explore the change of background and its consequence in detail. As the background modifies in the presence of extra force, the domain of the background also modifies depending on the strength of the force. The relevance of the size of the new domain is studied in §3. We write the Navier-Stokes equation for the modified background flow in the rotating frame,

as the primary plan is to the application in accretion disks, in §4 and also obtain the corresponding Reynolds number after nondimensionalizing it in §4.1. The perturbed flow equations have been formulated appropriately in the same section but in §4.2 where we recast the Navier-Stokes equation into Orr-Sommerfeld and Squire equations. Rotating Poiseuille and Couette-Poiseuille flows under purely vertical and three-dimensional perturbations are explored in detail in §5 and §6 respectively. Also how the stability of respective flows depends on the rotational profile is studied in the same sections. In §7, we describe the accuracy of our numerical results based on the technique we have used in this work. In §8, we compare plane Poiseuille flow with plane Couette flow in the presence of rotation. In the same section we also compare our critical parameters with those in literature. We finally conclude in §9 that depending on the boundary conditions and the strength of the extra force, there is a deviation in the flow from its linear shear nature. Further, rotation makes the flow unstable depending on the parameters and hence the flow plausibly becomes turbulent, which we suggest to be the hydrodynamical origin of turbulence in accretion disks.

## 2. BACKGROUND FLOW IN THE PRESENCE OF FORCE

Let us consider a very small cubical box of size  $L$  at a particular radius  $R_0$  from the center of the system as shown in the FIG. 1. At that radius, the box is rotating with an angular frequency  $\Omega_0$  such that  $\Omega = \Omega_0(R/R_0)^{-q}$  and the rotation parameter  $q = 3/2$  for Keplerian flow. In FIG. 1,  $S$  is the center of the box and the local analysis is done with respect to  $S$ . See Mukhopadhyay et al. 2005; Bhatia & Mukhopadhyay 2016; Ghosh & Mukhopadhyay 2020, for details of the reference frame and the background flow therein. Now let us set the local reference frame or box in such a way that the flow, which is along the  $\phi$ -direction with respect to  $C$ , to be in the  $y$ -direction and the motion of the either ends of the box in the  $x$ -direction (in the disk frame  $r$ -direction) to be with equal and opposite velocity of magnitude  $U_0$  (see fig. 1 of Ghosh & Mukhopadhyay 2020). In that local reference frame or box, the velocity of Keplerian flow becomes  $-q\Omega_0 X$  upto the first order approximation. This is the usual background flow (see Appendix A and also Hawley et al. 1995; Mukhopadhyay et al. 2005; Afshordi et al. 2005; Ghosh & Mukhopadhyay 2020) in the local region of an accretion disk. However, due to the presence of external force (may not be random) in the flow, the above-mentioned background flow is expected to change. The various possible origins of force in the system under consideration, as de-

scribed earlier by us (Ghosh & Mukhopadhyay 2020) in detail, could be: back reactions of outflow/jet to accretion disks, the interaction between the dust grains and fluid parcel in protoplanetary disks, etc. Using fluid-particle interactions, these possibilities could be modelled in such a way that the extra force turns out to be a function of the relative velocity between the fluid and the particles. For details, see section 2.1 and APPENDIX A of Ghosh & Mukhopadhyay (2020). In the presence of extra force, let us consider the background flow velocity to be  $\mathbf{V}$ , given by

$$\mathbf{V} = (0, V_Y(X), 0). \quad (1)$$

The corresponding Navier-Stokes equation describing the flow in the local box is

$$\frac{\partial \mathbf{V}}{\partial t} + (\mathbf{V} \cdot \nabla) \mathbf{V} = -\frac{\nabla P}{\rho} + \nu \nabla^2 \mathbf{V} + \mathbf{\Gamma}, \quad (2)$$

where  $P$ ,  $\rho$ ,  $\nu$  and  $\mathbf{\Gamma}$  are the pressure, density, kinematic viscosity and extra force respectively. The three components of equation (2) are

$$0 = -\frac{1}{\rho} \frac{\partial P}{\partial X} + \Gamma_X, \quad (3)$$

$$0 = -\frac{1}{\rho} \frac{\partial P}{\partial Y} + \nu \nabla^2 V_Y + \Gamma_Y, \quad (4)$$

$$0 = -\frac{1}{\rho} \frac{\partial P}{\partial Z} + \Gamma_Z. \quad (5)$$

Equation (4) can be further simplified to

$$\begin{aligned} \nabla^2 V_Y &= \frac{1}{\nu} \left( -\Gamma_Y + \frac{1}{\rho} \frac{\partial P}{\partial Y} \right) = \frac{\partial^2 V_Y}{\partial X^2} \\ \Rightarrow V_Y &= -\left( \frac{\Gamma_Y}{\nu} - \frac{1}{\nu \rho} \frac{\partial P}{\partial Y} \right) \frac{X^2}{2} + C_1 X + C_2 \\ &= -K \frac{X^2}{2} + C_1 X + C_2, \end{aligned} \quad (6)$$

where

$$K = \left( \frac{\Gamma_Y}{\nu} - \frac{1}{\nu \rho} \frac{\partial P}{\partial Y} \right), \quad (7)$$

is assumed to be constant.

The corresponding boundary conditions are given by

$$V_Y = \mp U_0 \text{ at } X = \pm L, \quad (8)$$

which imply that  $C_1 = -U_0/L$  and  $C_2 = KL^2/2$ . The background flow, therefore, in the presence of extra force modifies and it becomes

$$V_Y = \frac{K}{2}(L^2 - X^2) - \frac{U_0 X}{L}, \quad (9)$$

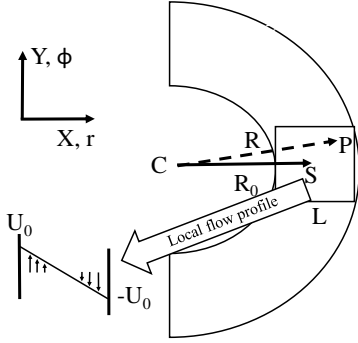


**Figure 1.** Schematic diagram of a shearing box centered at the point  $S$  inside the small patch of accretion disk. The box is of size  $L$ .  $C$  is the center of the accretion disk.  $S$  is at a distance  $R_0$  from  $C$ . An arbitrary fluid particle inside the box is at  $P$  at a distance  $R$  from  $C$ .

which is nothing but Couette-Poiseuille flow, when linear and nonlinear shears both are present. By a simple rearrangement, it reduces to

$$V_Y = \alpha (1 - \mathcal{X}^2), \quad (10)$$

where

$$\mathcal{X}^2 = \frac{K}{2} \frac{\Upsilon^2}{\alpha}, \quad \Upsilon^2 = \left( X + \frac{U_0}{KL} \right)^2 \quad (11)$$

$$\text{and } \alpha = \frac{U_0^2}{2KL^2} + \frac{L^2 K}{2}.$$

The velocity  $V_Y$  in equation (10) can be made dimensionless by dividing it with  $\alpha$ , i.e.

$$U_{\alpha Y} = \frac{V_Y}{\alpha} = 1 - \mathcal{X}^2, \quad (12)$$

where  $\alpha$  is the dimension of velocity, determined by the box geometry. The new background flow, therefore, becomes  $\mathbf{U}_\alpha = (0, U_{\alpha Y}, 0)$ . However, this is nothing but plane Poiseuille flow in new coordinates  $(\mathcal{X}, Y, Z)$ , where the boundary conditions are given by equation (8). Note that here  $\mathcal{X}$  is dimensionless, while  $Y$  and  $Z$  are dimensional coordinates. Nevertheless, it is useful to solve the problem within the known domain of the Poiseuille flow, i.e.  $\mathcal{X} \in [-1, 1]$ , in which it is known to be unstable above certain Reynolds number ( $Re$ ).

### 3. THE NEW DOMAIN

In order to employ the results of well-known Poiseuille flow, we set the boundary conditions in the new coordinates:  $\mathbf{U}_\alpha = 0$  at  $\mathcal{X} = \pm 1$ . It is therefore important to verify, the consequence of the domain of  $\mathcal{X}$  (i.e., running from -1 to 1) to the domain of  $X$  (i.e., running from  $-L$  to  $L$ ), as chosen originally. From equation (11), imposing  $\mathcal{X} = \pm 1$ , we have

$$X = \pm \sqrt{\frac{2\alpha}{K}} - \frac{U_0}{KL}, \quad (13)$$

where

$$\sqrt{\frac{2\alpha}{K}} = L \sqrt{\left( 1 + \frac{U_0^2}{K^2 L^4} \right)}. \quad (14)$$

Now if  $U_0^2/K^2 L^4 \ll 1$ , equation (14) shows that

$$\sqrt{\frac{2\alpha}{K}} \cong L + \frac{U_0^2}{2K^2 L^3}, \quad (15)$$

leading to

$$X = \pm L - \frac{U_0}{KL} \pm \frac{U_0^2}{2K^2 L^3}. \quad (16)$$

This confirms that the domain size of  $X$  is close to  $2L$  if  $U_0^2/K^2 L^4 \ll 1$ , i.e.  $\nu^2 U_0^2/L^4 \ll \Gamma_Y^2$ , when the flow is not driven by the pressure, i.e.  $\partial P/\partial Y = 0$ . However, in the presence of pressure gradient, the same condition will be true except its contribution will be added to the extra force.

However, if  $U_0^2/K^2 L^4 \gg 1$ , equation (14) shows that

$$\sqrt{\frac{2\alpha}{K}} \cong \frac{U_0}{KL}. \quad (17)$$

Hence

$$X = \pm \frac{U_0}{KL} - \frac{U_0}{KL}, \quad (18)$$

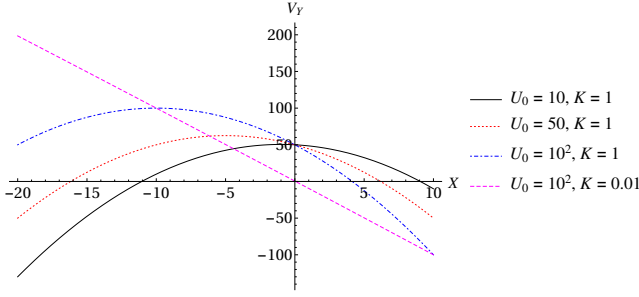
i.e. the domain size of  $X$  is approximately  $2U_0/KL$ . According to the approximation  $U_0^2/K^2 L^4 \gg 1$ ,  $2U_0/KL$  is much larger than  $2L$ . Hence, domain increases compared to what chosen originally. Therefore, our original choice of a small Cartesian patch in the flow may violate with this choice. This further may create problem for application to accretion disks, described below in detail.

FIG. 2 shows the modified background flow in the presence of constant extra force for various  $U_0$  and  $K$  with  $L = 10$ . It is clear that for  $U_0 = 10$  and  $K = 1$ , the new domain size almost remains same as  $2L = 20$ , because  $U_0^2/K^2 L^4 = 10^{-2} \ll 1$ . However, when  $U_0$  increases keeping  $K$  fixed, the domain size also increases. All these cases show the parabolic background flows in which the focus changes from  $(0, 0)$  to  $(-U_0/KL, 0)$ . Interestingly, if we keep decreasing  $K$  keeping  $U_0$  fixed, the linear background velocity eventually emerges again, as the extra force is negligible in this case (see equation 10).

The approximation  $U_0^2/K^2 L^4 \ll 1$  is, therefore, more suitable for our problem as it leads to almost the same domain size,  $2L$ , as chosen originally.

### 4. NAVIER-STOKES EQUATION IN ROTATING FRAME

Now our primary interest is to understand stability of rotating shear flows, particularly in the context of accretion disks. Hence, the plan is to examine the stability



**Figure 2.** Modification of the background flow in the presence of a constant extra force is shown against the flow variable  $X$  for various cases of parameters  $U_0$  and  $K$ , when  $L = 10$ .

of the background flow with velocity  $\mathbf{U}_\alpha$  within the new domain, i.e.  $\mathcal{X} \in [-1, 1]$ , as discussed in §3, which is rotating w.r.to the center of the system at  $R_0$ . Before doing so, we have to establish suitable equations depending on the reference frame and make them dimensionless for the convenience. This exploration is essentially the stability analysis of plane Poiseuille flow in the presence of rotation, here particularly the Coriolis effect. In the due process, we obtain a dimensionless number characterizing the flow to be laminar or turbulent in the domain of interest, i.e. the Reynolds number in the new coordinate system  $(\mathcal{X}, Y, Z)$  which is  $Re_\alpha$ .

#### 4.1. Defining Reynolds number in a local region

Let us consider the local Cartesian frame or box at radius  $R_0$ , as shown by FIG. 1, rotating with the angular velocity  $\boldsymbol{\omega} = (0, 0, \Omega_0)$  such that  $\Omega = \Omega_0(R/R_0)^{-q}$ , where  $\Omega_0 = V_Y(\mathcal{X} = 0)/(qL_{ch}/2) = 2\alpha\sqrt{K}/q\sqrt{2\alpha} = \alpha\sqrt{2K}/q\sqrt{\alpha}$ ,  $L_{ch}$  is the characteristic length scale of the system. The Navier-Stokes equation in that frame is

$$\frac{\partial \mathbf{V}}{\partial t'} + (\mathbf{V} \cdot \nabla) \mathbf{V} + \boldsymbol{\omega} \times \boldsymbol{\omega} \times \mathbf{D} + 2\boldsymbol{\omega} \times \mathbf{V} + \frac{\nabla P}{\rho} = \nu \nabla^2 \mathbf{V} + \boldsymbol{\Gamma}, \quad (19)$$

where the position vector  $\mathbf{D} = (X, Y, Z)$ , and  $\nabla = (\partial/\partial X, \partial/\partial Y, \partial/\partial Z)$  in Cartesian coordinates. If we divide both sides of equation (19) by  $\alpha$ , we obtain an equation for  $\mathbf{U}_\alpha$ , which is given by

$$\frac{\partial \mathbf{U}_\alpha}{\partial t'} + \alpha(\mathbf{U}_\alpha \cdot \nabla) \mathbf{U}_\alpha + \boldsymbol{\omega} \times \boldsymbol{\omega} \times \frac{\mathbf{D}}{\alpha} + 2\boldsymbol{\omega} \times \mathbf{U}_\alpha + \nabla P_\alpha = \nu \nabla^2 \mathbf{U}_\alpha + \boldsymbol{\Gamma}_\alpha, \quad (20)$$

where  $P_\alpha = P/\rho\alpha$  and  $\boldsymbol{\Gamma}_\alpha = \boldsymbol{\Gamma}/\alpha$ . We now redefine the variables in terms of dimensionless quantities, i.e.  $t' \rightarrow \sqrt{2/\alpha K}t$ ,  $(X, Y, Z) \rightarrow \sqrt{2\alpha/K}(\mathcal{X}, y, z)$ , where  $\mathbf{d} = (\mathcal{X}, y, z)$ , and  $\nabla \rightarrow \sqrt{K/2\alpha}\nabla_\alpha$ , where  $\nabla_\alpha = (\partial/\partial \mathcal{X}, \partial/\partial y, \partial/\partial z)$ . Hence, equation (20) in terms of dimensionless variables, for incompressible fluid, be-

comes

$$\frac{\partial \mathbf{U}_\alpha}{\partial t} + (\mathbf{U}_\alpha \cdot \nabla_\alpha) \mathbf{U}_\alpha + \frac{1}{q^2} \hat{k} \times \hat{k} \times \mathbf{d} + \frac{2}{q} \hat{k} \times \mathbf{U}_\alpha + \frac{1}{\alpha} \nabla_\alpha P_\alpha = \frac{\nu \sqrt{K}}{\alpha \sqrt{2\alpha}} \nabla_\alpha^2 \mathbf{U}_\alpha + \boldsymbol{\Gamma}'_\alpha. \quad (21)$$

The Reynolds number, therefore, is defined as

$$Re_\alpha = \frac{\alpha \sqrt{2\alpha}}{\nu \sqrt{K}} \quad (22)$$

and  $\boldsymbol{\Gamma}'_\alpha = \boldsymbol{\Gamma} \sqrt{2/K\alpha^3}$ .

#### 4.2. Perturbation analysis

Equation (21) along with

$$\nabla_\alpha \cdot \mathbf{U}_\alpha = 0 \quad (23)$$

describes the dynamics of fluid inside the local box. Now we perturb equations (21) and (23) linearly and check whether the perturbation decays or grows with time. The velocity perturbation is  $\mathbf{u}' = (u, v, w)$ , the corresponding vorticity perturbation is  $\nabla \times \mathbf{u}'$  and the pressure perturbation is  $p'$ . After perturbing equation (21), we eliminate the pressure term from the governing equation and recast it into the corresponding homogeneous Orr-Sommerfeld and Squire equations, which are given by

$$\left( \frac{\partial}{\partial t} + U_{\alpha Y} \frac{\partial}{\partial y} \right) \nabla_\alpha^2 u - U_{\alpha Y}'' \frac{\partial u}{\partial y} + \frac{2}{q} \frac{\partial \zeta}{\partial z} - \frac{1}{Re_\alpha} \nabla_\alpha^4 u = 0, \quad (24)$$

$$\left( \frac{\partial}{\partial t} + U_{\alpha Y} \frac{\partial}{\partial y} \right) \zeta - U_{\alpha Y}' \frac{\partial u}{\partial z} - \frac{2}{q} \frac{\partial u}{\partial z} - \frac{1}{Re_\alpha} \nabla_\alpha^2 \zeta = 0, \quad (25)$$

where  $\zeta$  is the  $x$ -components of the vorticity perturbations, prime denotes the differentiation w.r.to  $\mathcal{X}$  and the extra force  $\boldsymbol{\Gamma}$  is assumed to remain same under perturbation so that it gets eliminated from the equation. If  $\boldsymbol{\Gamma}$  would have considered to be changed under perturbation, it would create additional impact into the flow in order to reveal instability, as discussed by us recently (Ghosh & Mukhopadhyay 2020) in the context of linear shear. However, for the present purpose, we plan to explore minimum impact of force onto the flow. Nevertheless, equations (24) and (25) are the homogeneous part of the Orr-Sommerfeld and Squire equations corresponding to the perturbation to the equation (21)

(see Ghosh & Mukhopadhyay 2020, for inhomogeneous Orr-Sommerfeld and Squire equations due to the effect of force). The corresponding chosen no-slip boundary conditions are:  $u = v = w = 0$  at the two boundaries  $\mathcal{X} = \pm 1$ , or equivalently  $u = \frac{\partial u}{\partial \mathcal{X}} = \zeta = 0$  at  $\mathcal{X} = \pm 1$ . Hence, the linearized eigenspectra corresponding to equation (21) will be described by equations (24) and (25) only. The eigenspectra will not change due to the presence of the nonhomogeneous term arising due to the presence of the extra force. Our main aim here is to observe the changes in the eigenspectra, because of the changes in various flow properties. Note importantly that in principle a small section of an accretion disk should not have any boundary, as imposed here in order to introduce the boundary condition for the solution purpose. However, the idea is that the entire disk, at least the region where turbulence is sought of, is divided into small boxes and if one box is unstable under perturbation, others will do so. All boxes are assumed to be arranged together. Hence, on either side of a boundary, the perturbation remains working intact in the respective boxes. Therefore, although boundaries are introduced for the solution purpose, it does not practically introduce any artifact for the present purpose. Nevertheless, Mukhopadhyay et al. (2005) and Afshordi et al. (2005) showed that results practically do not depend on whether the analyses are based on the shearing sheet or shearing box.

## 5. PERTURBATION ANALYSIS OF ROTATING POISEUILLE FLOW

### 5.1. Three-dimensional perturbation

In order to understand the evolution of linear perturbation, let the linear solutions be (e.g. Mukhopadhyay et al. 2005)

$$u = \hat{u}(\mathcal{X}, t)e^{i\mathbf{k}\cdot\mathbf{r}}, \quad (26)$$

$$\zeta = \hat{\zeta}(\mathcal{X}, t)e^{i\mathbf{k}\cdot\mathbf{r}}, \quad (27)$$

with  $\mathbf{k} = (0, k_y, k_z)$  and  $\mathbf{r} = (0, y, z)$ . Substituting these in equations (24) and (25), neglecting non-linear terms, we obtain

$$\begin{aligned} \frac{\partial \hat{u}}{\partial t} + i(\mathcal{D}^2 - k^2)^{-1} \left[ k_y U_{\alpha Y} (\mathcal{D}^2 - k^2) - k_y U''_{\alpha Y} \right. \\ \left. - \frac{1}{iRe_\alpha} (\mathcal{D}^2 - k^2)^2 \right] \hat{u} + (\mathcal{D}^2 - k^2)^{-1} \frac{2}{q} i k_z \hat{\zeta} = 0. \end{aligned} \quad (28)$$

and

$$\frac{\partial \hat{\zeta}}{\partial t} + i k_y U_{\alpha Y} \hat{\zeta} - \left( U'_{\alpha Y} + \frac{2}{q} \right) i k_z \hat{u} - \frac{1}{Re_\alpha} (\mathcal{D}^2 - k^2) \hat{\zeta} = 0, \quad (29)$$

where  $\mathcal{D} = \frac{\partial}{\partial \mathcal{X}}$ .

Further combining equations (28) and (29) we obtain

$$\frac{\partial}{\partial t} Q + i\mathcal{L}Q = 0, \quad (30)$$

where

$$Q = \begin{pmatrix} \hat{u} \\ \hat{\zeta} \end{pmatrix}, \quad \mathcal{L} = \begin{pmatrix} \mathcal{L}_{11} & \mathcal{L}_{12} \\ \mathcal{L}_{21} & \mathcal{L}_{22} \end{pmatrix}, \quad (31)$$

$$\begin{aligned} \mathcal{L}_{11} &= (\mathcal{D}^2 - k^2)^{-1} \left[ k_y U_{\alpha Y} (\mathcal{D}^2 - k^2) - k_y U''_{\alpha Y} \right. \\ &\quad \left. - \frac{1}{iRe_\alpha} (\mathcal{D}^2 - k^2)^2 \right], \\ \mathcal{L}_{12} &= \frac{2k_z}{q} (\mathcal{D}^2 - k^2)^{-1}, \\ \mathcal{L}_{21} &= - \left( U'_{\alpha Y} + \frac{2}{q} \right) k_z, \\ \mathcal{L}_{22} &= k_y U_{\alpha Y} - \frac{1}{iRe_\alpha} (\mathcal{D}^2 - k^2), \end{aligned} \quad (32)$$

Now the solution of the equation (30) is given by

$$Q = \sum_{m=1}^{\infty} C_m Q_{\mathcal{X},m}(\mathcal{X}) \exp\{-i\sigma_m t\}, \quad (33)$$

where index  $m$  corresponds to the combined Orr-Sommerfeld and Squire modes and  $Q_{\mathcal{X},m}(x)$  satisfies the eigenvalue equation

$$\mathcal{L}Q_{\mathcal{X},m}(\mathcal{X}) = \sigma_m Q_{\mathcal{X},m}. \quad (34)$$

Here  $\sigma$  is a complex quantity, given by  $\sigma = \sigma_r + i\sigma_i$ . In this article,  $\sigma_r$ ,  $\sigma_i$  and hence  $\sigma$  for different parameters and different flows are obtained numerically. The numerical method for discretization is described in §7.

It is well-known that Poiseuille flow is linearly unstable under twodimensional perturbation with  $k_y = 1.02$  and  $k_z = 0$  and the critical  $Re$  is about 5772.22. However for the same  $Re$ , this flow is stable under perturbation with  $k_y = k_z = 1$ . Nevertheless, in the presence of Keplerian rotation of the whole system, i.e. due to the effect of Coriolis force in the local rotating box, the situation changes. FIG. 3 shows the eigenspectra for linearly perturbed Poiseuille flow in the rotating frame (while the small region under consideration is rotating) with  $q = 1.5$  (Keplerian rotation) for  $k_y = k_z = 1$  for different  $Re_\alpha$ . Here we observe that while the flow is stable for  $Re_\alpha = 100$  and 1000 with  $k_y = k_z = 1$ , it is unstable for  $Re_\alpha = 10000$ . FIG. 4 also depicts the eigenspectra for the same flow as in FIG. 3 but for  $Re_\alpha = 6000$  and 7000. It confirms that instability arises between for  $Re_\alpha = 6000$  and 7000. The critical  $Re_\alpha$  is around 6431.473. FIG. 5 depicts a sample of velocity

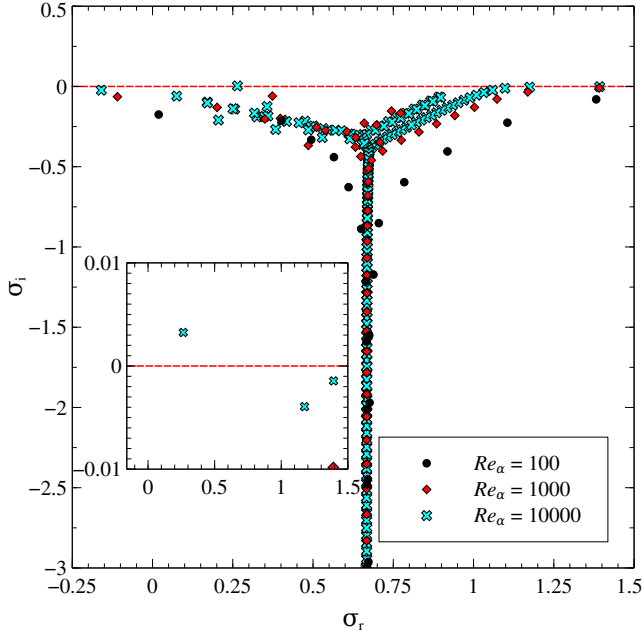


**Figure 3.** Eigenspectra for linearized Poiseuille flow in the presence of Keplerian rotation ( $q = 1.5$ ) of the box for  $Re_\alpha = 100, 1000$  and  $10000$ , with  $k_y = k_z = 1$ .

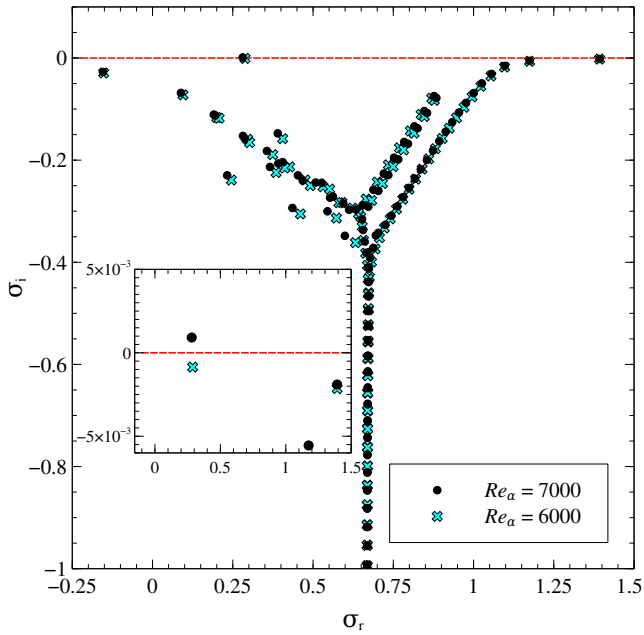


**Figure 4.** Same as 3, except for  $Re_\alpha = 6000$  and  $7000$ .

eigenfunction, which is given here for the most unstable mode corresponding to Poiseuille flow for  $Re_\alpha = 7000$ ,  $k_y = k_z = 1$ , and  $q = 1.5$ .

Depending on the localization of eigenfunctions, the corresponding modes are named. If the eigenfunctions have their maxima around the center of the domain,

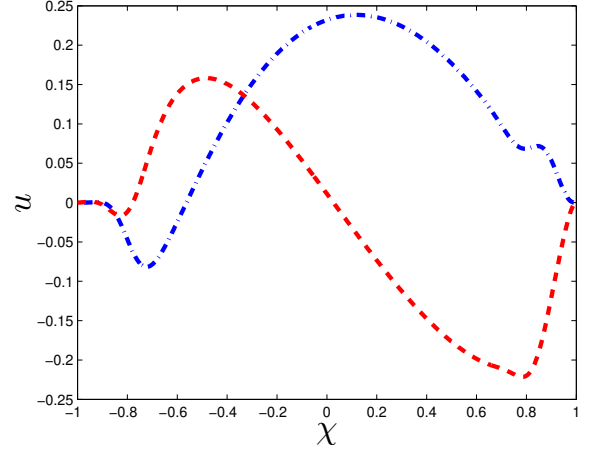


**Figure 5.** Velocity eigenfunction for the most unstable mode corresponding to linearized Poiseuille flow in the presence of Keplerian rotation ( $q = 1.5$ ) of the box for  $Re_\alpha = 7000$  with  $k_y = k_z = 1$ . Dot-dashed and dashed lines indicate, respectively, the real and imaginary parts of  $u$ .

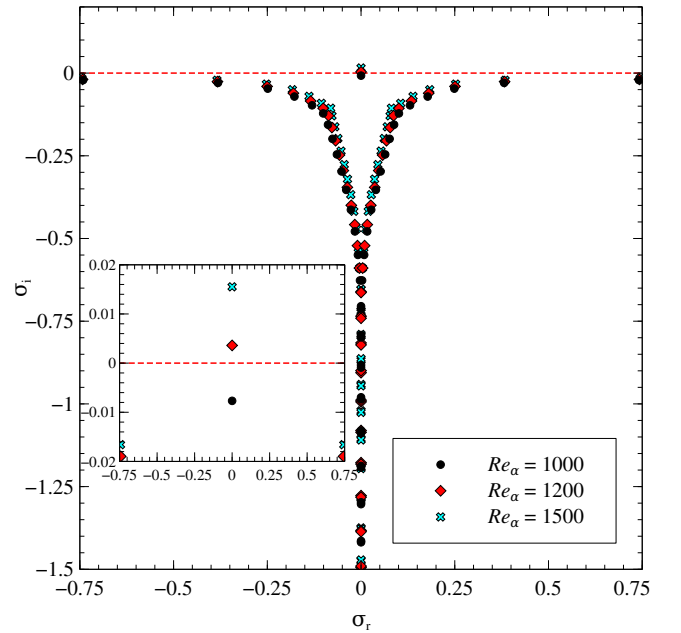


**Figure 6.** Eigenspectra for linearized Poiseuille flow in the presence of Keplerian rotation ( $q = 1.5$ ) of the box for  $Re_\alpha = 1000, 1200$  and  $1500$ , with a pure vertical perturbation, i.e.  $k_y = 0$  and  $k_z = 1$ .

the corresponding modes are called body modes. If the eigenfunctions are localized around the boundary, the corresponding modes are called wall modes. See [Kersale et al. \(2004\)](#) for details about these modes. From FIG. 5, we see that the modes are body modes.

We have imposed no-slip boundary conditions to obtain all the eigenspectra corresponding to Poiseuille

flow in the presence of rotation. However, for different boundary conditions, the unstable nature of the flow does not disappear from the system. Xiong & Tao (2020) argued that with the change of boundary conditions, only the critical Reynolds number and other parameters revealing instability change.

To have a qualitative sense of why plane Poiseuille flow in the presence of Keplerian rotation becomes unstable under threedimensional perturbation unlike the nonrotating case, below we investigate the effect of pure vertical perturbation.

### 5.2. Pure vertical perturbation

We consider pure vertical perturbation of the form  $u, \zeta \sim u(t), \zeta(t) \exp(ik_z z)$  for the ease of analytical exploration and hence equations (24) and (25) reduce to respectively

$$\frac{\partial u}{\partial t} - \frac{2i}{qk_z} \zeta = -\frac{1}{Re_\alpha} k_z^2 u \quad (35)$$

and

$$\frac{\partial \zeta}{\partial t} - ik_z \left( \frac{2}{q} + U'_{\alpha Y} \right) u = -\frac{1}{Re_\alpha} k_z^2 \zeta. \quad (36)$$

Note, however, that this is just for the sake of an approximate analytical exploration, as due to shear in the  $x$ -direction, the perturbation cannot have this form, as we even did not choose it in our exploration of eigen-spectrum analysis. Combining equations (35) and (36), we obtain a second order temporal differential equation for  $u(t)$ , given by

$$\frac{\partial^2 u}{\partial t^2} + \frac{2k_z^2}{Re_\alpha} \frac{\partial u}{\partial t} + \left( \frac{4}{q^2} + \frac{2U'_{\alpha Y}}{q} + \frac{k_z^4}{Re_\alpha^2} \right) u = 0. \quad (37)$$

Let us consider the solution of equation (37) be  $u(t) \sim \exp(\sigma t)$ ,  $\gamma = 2k_z^2/Re_\alpha$  and  $\beta = 4/q^2 + 2U'_{\alpha Y}/q + k_z^4/Re_\alpha^2$ . Hence from equation (37), we obtain a quadratic equation for  $\sigma$ , given by

$$\sigma^2 + \gamma\sigma + \beta = 0, \quad (38)$$

whose solution is

$$\sigma = -\frac{\gamma}{2} \pm \sqrt{-\frac{4}{q^2} - \frac{2U'_{\alpha Y}}{q}}. \quad (39)$$

If the background flow follows the equation (12), then equation (39) becomes

$$\sigma = -\frac{\gamma}{2} \pm 2\sqrt{\frac{\mathcal{X}}{q} - \frac{1}{q^2}}. \quad (40)$$

From the above equation, it is clear that whenever the quantity under the root is real positive, one of the solutions for the vertical perturbation may grow with time

exponentially. This depends on whether the magnitude of the term involved with square root (second term) is greater or less than the first term. As  $\mathcal{X}$  varies between  $-1$  and  $+1$ , it is very obvious that the vertical perturbation will grow for the system under consideration. However as the growing modes correspond to a real positive  $\sigma_i$ , there is a lower bound of  $\mathcal{X}$  for the modes to be confined in the system.

FIG. 6 shows, by full numerical solutions, the eigen-spectra for the Poiseuille flow in the presence of Keplerian rotation in the case of pure vertical perturbation, i.e.  $k_y = 0$  and  $k_z = 1$ , for  $Re_\alpha = 1000, 1200$  and  $1500$ . From the inset figure, it is very clear that the flow is stable for  $Re_\alpha = 1000$ . However, it is unstable for  $Re_\alpha = 1200$  and  $1500$  and the critical  $Re_\alpha$  is around  $1129.18$ .

Above results argue that for an astrophysical accretion disk, when the flow is necessarily threedimensional with rotation, a very small force makes the system unstable as its  $Re$  is huge (see, e.g., Mukhopadhyay 2013). Even if  $\partial P/\partial Y$  vanishes, a finite  $\Gamma_Y/\nu \equiv Re_\alpha \Gamma_Y$  would suffice for instability due to the emergence of small contribution of  $x^2$  (Poiseuille) effect along with  $x$  (Couette) effect in the background. In fact at large  $U_0$ , when the quadratic term in  $X$  in equation (9) is small compared to the linear term in  $X$ ,  $Re_\alpha \rightarrow \nu U_0^3/2L^3\Gamma_Y^2$ . Therefore, a very small force  $\Gamma_Y$  along with a similar small  $\nu$  would suffice a huge  $Re_\alpha$ , which might lead to linear instability and subsequent nonlinearity and turbulence in accretion disks. In plane Couette flow in laboratory, when  $\nu$  is not very small, still a small force would lead to instability and turbulence at large  $U_0$ . For an intermediate  $U_0$ , the instability is expected to arise at an intermediate  $Re_\alpha$ , as seen in experiments. The above arguments remain intact if the force is solely due to the unavoidable pressure gradient, whether tiny or not, such that  $K = 1/(\nu\rho)\partial P/\partial Y$ . We will discuss in detail the relative importance of external force and background velocity along with viscosity in order to control flow stability in §6 below.

### 5.3. Dependence of the stability on rotation profile

In the last two subsections, we have observed how the Keplerian rotation affects the threedimensional and vertical perturbations. Here, we shall observe how the stability of plane Poiseuille flow depends on rotation profile, i.e. on different  $q$ . FIG. 7 describes the eigenspectra of Poiseuille flow for three different rotational profiles under a purely vertical perturbation. Here we notice that for a fixed  $Re_\alpha$ , larger  $q$  has larger growth rate. In addition, we notice that while  $q = 1$  provides stable flow, the other three chosen  $q$  result in unstable flow. For a three



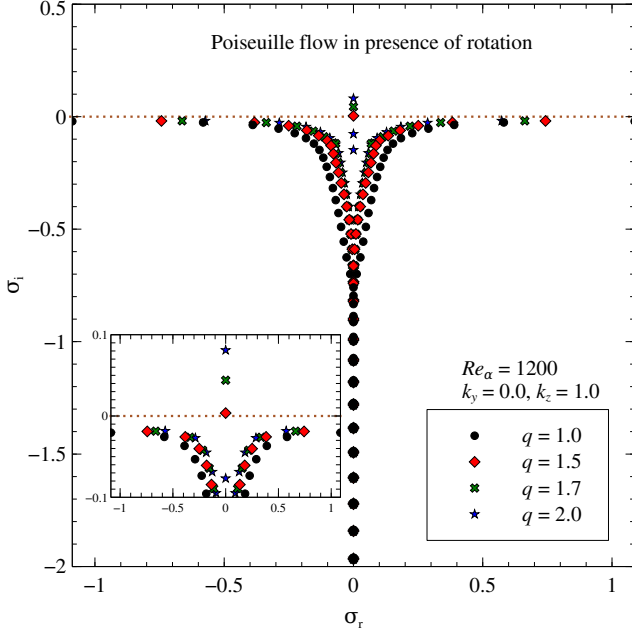


**Figure 7.** Eigenspectra of linearized Poiseuille flow in the presence of rotation for vertical perturbation with  $k_y = 0$  and  $k_z = 1$  for four different  $q$  and  $Re_\alpha = 1200$ .

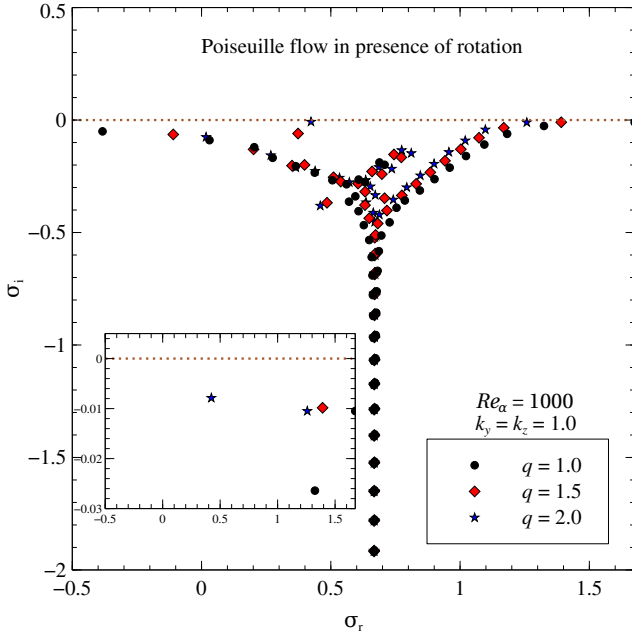


**Figure 8.** Eigenspectra of linearized Poiseuille flow in the presence of rotation for three-dimensional perturbation with  $k_y = k_z = 1$  for three different  $q$  and  $Re_\alpha = 1000$ .

dimensional perturbation (i.e.  $k_y$  and  $k_z$  both nonzero) also stability decreases with increasing  $q$ , as is evident from FIG. 8. However, as opposed to the purely vertical perturbation, in the three-dimensional case, flows of all  $q$  are stable, for the chosen set of parameters.

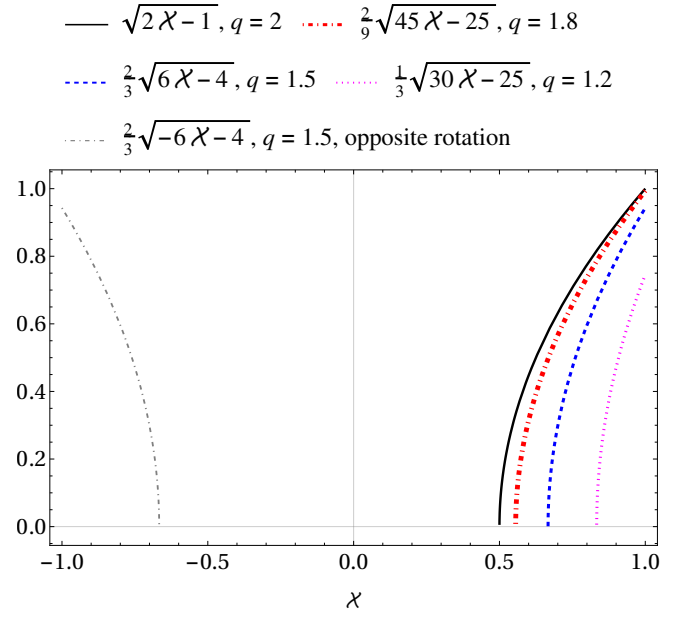


**Figure 9.** Variation of  $2\sqrt{\mathcal{X}/q - 1/q^2}$  from equation (40) as a function of  $\mathcal{X}$  for  $q = 1.2, 1.5, 1.8, 2.0$  and for a oppositely rotating flow with  $q = 1.5$ .

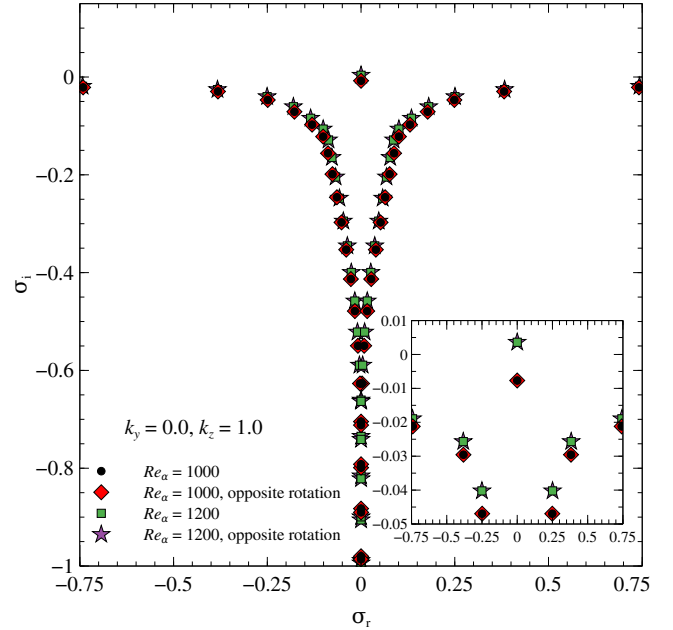


**Figure 10.** Eigenspectra of linearized Poiseuille flow in the presence of rotation for vertical perturbation with  $k_y = 0$ , and  $k_z = 1$  for  $Re_\alpha$ , but for two opposite orientations of Keplerian rotation.

Let us understand this fact from equation (40). We consider two extreme cases of  $q$ , i.e.  $q = 1$  and  $q = 2$ . Equation (40) for these two cases become

$$\sigma = -\frac{\gamma}{2} \pm 2\sqrt{\mathcal{X} - 1} \quad (41)$$

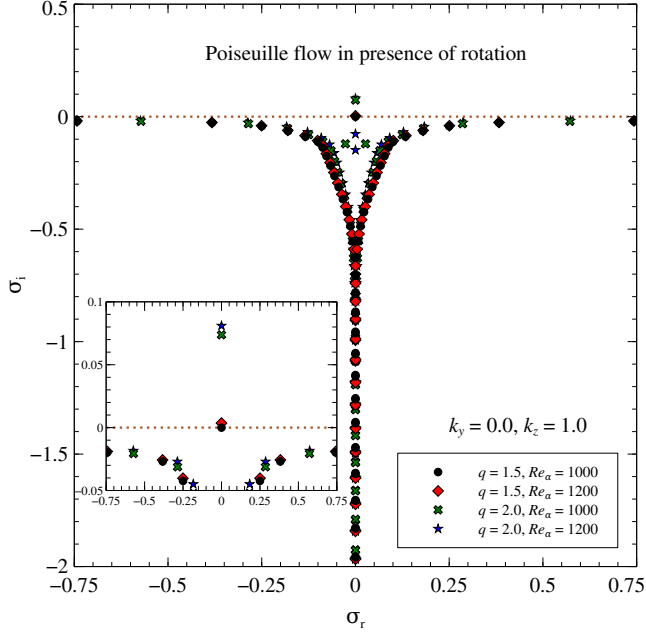


**Figure 11.** Eigenspectra of linearized Poiseuille flow in the presence of rotation for vertical perturbation with  $k_y = 0$ , and  $k_z = 1$  for two different  $q$  and  $Re_\alpha$ .

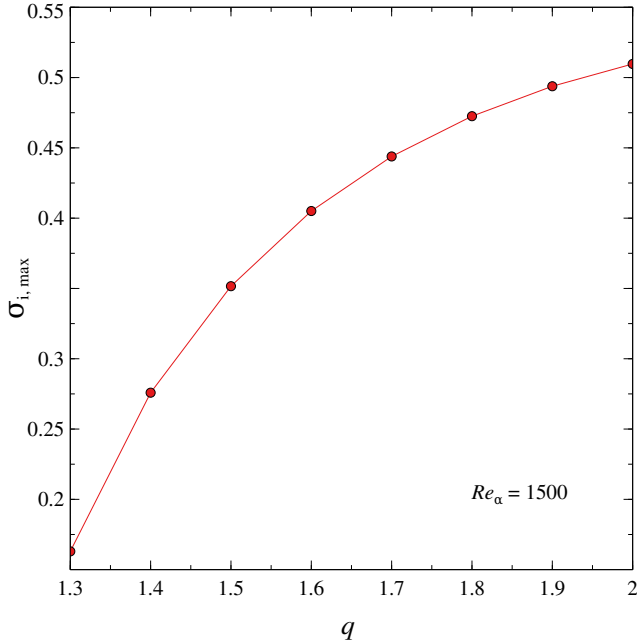


**Figure 12.** Maximum growth rate ( $\sigma_{i, max}$ ) as a function of  $q$  in linearized Poiseuille flow for vertical perturbation with those  $k_z$  giving rise to  $\sigma_{i, max}$  for  $Re_\alpha = 1500$ .

and

$$\sigma = -\frac{\gamma}{2} \pm \sqrt{2\mathcal{X} - 1} \quad (42)$$

respectively. From equation (41), we can obtain that the system will be unstable if  $(\mathcal{X} - 1)$  is a positive real

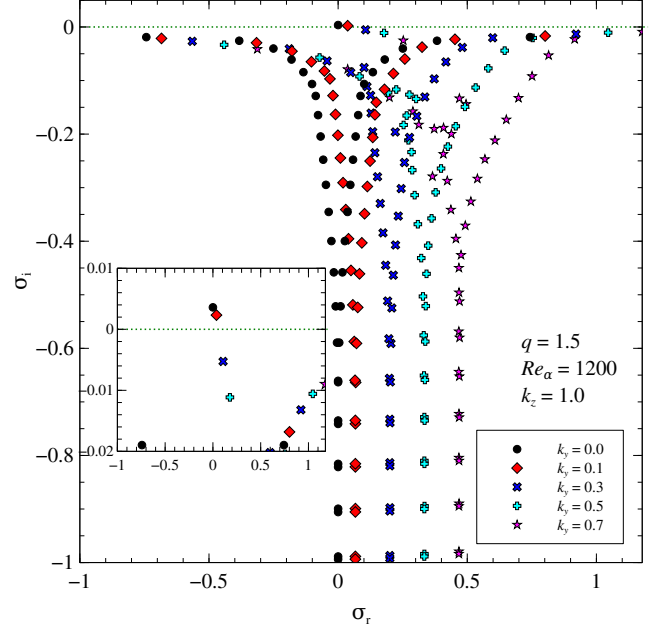


**Figure 13.** Eigenspectra of linearized Poiseuille flow in the presence of Keplerian rotation for perturbations with  $k_z = 1$  but with five different  $k_y$  for  $Re_\alpha = 1200$ .

number and

$$\sqrt{\mathcal{X} - 1} > \frac{\gamma}{4} = \frac{k_z^2}{2Re_\alpha}. \quad (43)$$

Now,  $(\mathcal{X} - 1)$  is negative other than at  $\mathcal{X} = 1$  as  $\mathcal{X} \in [-1, 1]$ . However at  $\mathcal{X} = 1$ , equation (43) is also not valid there as  $k^2/Re_\alpha > 0$  always. Therefore, plane Poiseuille flow with  $q = 1$  will always be stable. It explains the reason behind the stable Poiseuille flow with vertical perturbations for  $q = 1$  as depicted in the FIG. 7.

To make the system unstable for  $q = 2$ , from equation (42), we require  $(2\mathcal{X} - 1)$  to be a positive real number and

$$\sqrt{2\mathcal{X} - 1} > \frac{\gamma}{2} = \frac{k_z^2}{Re_\alpha}. \quad (44)$$

Now  $(2\mathcal{X} - 1)$  could be positive within the domain of  $\mathcal{X}$ . Hence, for  $q = 2$ , plane Poiseuille flow will be unstable depending on the parameters, i.e.  $k_z$  and  $Re_\alpha$ .

Now for a general  $q$  (usually  $1 \leq q \leq 2$  for the present interest), to make the system unstable,  $\mathcal{X}/q - 1/q^2$  has to be a positive real number and also from equation (40)

$$2\sqrt{\frac{\mathcal{X}}{q} - \frac{1}{q^2}} > \frac{\gamma}{2} = \frac{k_z^2}{Re_\alpha}. \quad (45)$$

It is important to check in which domain of  $\mathcal{X}$ ,  $\mathcal{X}/q - 1/q^2$  is positive and equation (45) satisfies. Moreover, it is also important to know how the maximum growth

rates for vertical perturbations depend on  $q$ . The answers to these queries can be found in FIG. 9, where the variation of  $2\sqrt{\mathcal{X}/q - 1/q^2}$  as a function of  $\mathcal{X}$  is shown for five different  $q$ . It shows that the size of the domain, in which  $2\sqrt{\mathcal{X}/q - 1/q^2}$  remains a real number and hence  $(\mathcal{X}/q - 1/q^2)$  remains a positive real number, decreases as  $q$  decreases. From equation (40), it is obvious that the maximum growth rates will be larger for those  $q$ 's for which  $2\sqrt{\mathcal{X}/q - 1/q^2}$  will be larger. From FIG. 9, we notice that as  $q$  decrease,  $2\sqrt{\mathcal{X}/q - 1/q^2}$  also decreases. This reveals that larger  $q$  will have larger growth rates with a larger domain. This explains the reason behind the larger growth rates (less stability) for vertical (threedimensional) perturbations for larger  $q$  for a fixed  $Re_\alpha$ .

Interestingly, above findings argue for a striking similarities between the Papaloizou-Pringle instability (PPI, see e.g. Papaloizou & Pringle 1984; Balbus 2003) and the instability that we have obtained here, specifically the one with the vertical perturbations. For PPI, the pressure gradient is nonzero in the equilibrium. In our case, we also consider a modified background due to the presence of pressure gradient and/or an external force in the local frame. For PPI, the perturbations have to be non-axisymmetric. These non-axisymmetric perturbations contain the information of rotation (Balbus 2003). However, in our case, it is the vertical perturbation that couples with the rotation, playing an important role to reveal (faster) instability. Our vertical perturbation is, therefore, equivalent to the non-axisymmetric perturbations required for PPI.

Now importantly the sign of the terms involved with  $q$  (but not  $q$  itself) in the equations can be both positive and negative. The negative sign implies the opposite sense of rotation as compared to the positive sign. FIG. 10 shows that the eigenspectra for plane Poiseuille flow in the presence of rotation with either of the orientations for a vertical perturbation. We notice that the eigenspectra are identical for both the orientations of Keplerian rotation for a fixed  $Re_\alpha$ . From equation (40) and FIG. 9, it is obvious that the negative rotational effect (when the term involved with  $1/q$  is negative) gets nullified by the negativity of  $\mathcal{X}$ , which is equivalent to the positive rotational effect in the positive  $\mathcal{X}$  region. Hence, for the entire zone of  $\mathcal{X}$ , the net effect appears to be unchanged in either of the orientations of rotation. This explains why eigenspectra are independent of the orientation of rotation for a vertical perturbation. Nevertheless, for threedimensional perturbation also, this conclusion is true. The reason is the following. In order to obtain the eigenspectra, we should have the secular determinant corresponding to the operator  $\mathcal{L}$  in equa-

tion (31). The information of rotation enters into the picture by  $\mathcal{L}_{12}$  and  $\mathcal{L}_{21}$ . In that secular equation,  $\mathcal{L}_{12}$  and  $\mathcal{L}_{21}$  appear as multiplication between themselves. More interestingly, we notice that

$$\mathcal{L}_{12}\mathcal{L}_{21} = \left(\frac{\mathcal{X}}{q} - \frac{1}{q^2}\right) 4k_z^2(\mathcal{D}^2 - k^2)^{-1}. \quad (46)$$

$\mathcal{L}_{12}\mathcal{L}_{21}$ , therefore, does not depend on the orientation of rotation because of the presence of  $\mathcal{X}$  which spans from  $-1$  to  $+1$ .

We also can obtain the domain of  $q$  which could give rise to instability depending on other parameters. From equation (40), the first condition for instability, irrespective of the orientation of rotation, is

$$\frac{\mathcal{X}}{q} - \frac{1}{q^2} > 0, \quad (47)$$

or in other words

$$\mathcal{X} > \frac{1}{q}. \quad (48)$$

For the flows with  $q < 1$  (when  $q$  is positive for the present purpose), the above condition violates. Hence, our primary domain of  $q$  for the plausible unstable flows in the present context is  $q < \infty$  excluding the domain  $q \in [0, 1]$ . However, in the present context the domain of interest is  $q \in [1, 2]$  and  $q \rightarrow \infty$  (conventional plane Couette flow without rotation).

FIG. 11 describes the eigenspectra for plane Poiseuille flow in the presence of rotation for a vertical perturbation to capture two phenomena. In one hand, it shows that for a fixed  $q$ , increment of  $Re_\alpha$  increases the growth rates of a vertical perturbation. On the other hand, it also depicts that the increment of  $q$  for a fixed  $Re_\alpha$ , increases the growth rates of a vertical perturbation. However, the latter has more stronger effect than the earlier. This is because when we observe the flow for a fixed  $q$  but at different  $Re_\alpha$ 's, we observe the same flow at different levels of initial velocity (lower  $Re_\alpha$  corresponds to a more streamline flow). However, for different  $q$ 's, we altogether study the different flows, when the stronger rotation is more prone to instability.

FIG. 12 describes the variation of maximum growth rate ( $\sigma_{i,max}$ ) as a function of  $q$  for vertical perturbation with  $Re_\alpha = 1500$ . Here the growth rates are maximized over the wavenumbers,  $k_z$ , i.e., we consider those  $k_z$ 's, which give rise to the maximum growth rate corresponding to each  $q$ . FIG. 12 further shows that  $\sigma_{i,max}$  increases with increasing  $q$ , which can be understood qualitatively from FIG. 9 and equation (40).

FIG. 13 describes eigenspectra of plane Poiseuille flow in the presence of rotation for five different  $k_y$ . Interestingly, here we notice that as  $k_y$  increases (i.e. the perturbation becomes more threedimensional from purely

vertical in nature), the flow becomes more and more stabilized, or the unstable flow becomes stable. As we have already mentioned earlier that plane Poiseuille flow becomes unstable at a  $Re = 5772.22$  for planer (i.e.  $k_z = 0.0$ ) perturbation. However, we have seen in the previous subsections and also we shall discuss in §8 that rotational effect makes the flow unstable at a  $Re$  which is about two orders of magnitude lesser than that obtained based on a planer perturbation. For plane Poiseuille flow, therefore, the rotational effect (or the corresponding Coriolis effect) is more prone to lead to instability than that from Tollmien-Schlichting waves (Alfredsson & Persson 1989), which are the corresponding planer perturbation modes at the critical  $Re$ . See further §6.2 to understand other detailed physics behind the eigen-spectra.

## 6. PERTURBATION ANALYSIS TO ROTATING COUETTE-POISEUILLE FLOW

### 6.1. The formulation of dimensionless background flow

As shown in §2, plane Couette flow in the presence of external force develops a nonlinear shear in addition to its background linear shear, as shown by equation (9). This is called Couette-Poiseuille flow. Of course in a suitable coordinate frame, plane Couette-Poiseuille flow will turn out to be plane Poiseuille flow as shown in equation (10). Nevertheless, as shown by FIG. 2, depending upon the flow parameters, i.e. strength of force and background velocity, the domain of plane Poiseuille flow, more precisely plane Couette-Poiseuille flow, varies which further affects the flow behavior under perturbation. Here, we explore Couette-Poiseuille flow under various flow parameters. We, therefore, have to make the equation (9) dimensionless. In dimensionless units, equation (9) turns out to be

$$U = \xi(1 - x^2) - x, \quad (49)$$

where  $\xi = KL^2/2U_0 = \Gamma_Y L^2/2\nu U_0$  and  $x = X/L$ . The background velocity vector, therefore, is  $\mathbf{U} = (0, U, 0)$ .

To examine the stability of the background flow with velocity  $\mathbf{U}$  within the domain,  $x \in [-1, 1]$ , in a rotating frame at  $R_0$ , we consider the same prescription of angular velocity of the rotating frame as chosen in §4.1, given by  $\boldsymbol{\omega} = (0, 0, \Omega_0)$ ,  $\Omega = \Omega_0(R/R_0)^{-q}$ , and  $\Omega_0 = U_0/qL$ . Although the similar kind of flow was explored by Balakumar (1997), they did not consider the effect of rotation which is crucial for astrophysical bodies particularly for accretion disks. Following the same procedure as done in §4.1, particularly from equations (19) to (22), we can redefine the Reynolds number corresponding to the flow as

$$Re = \frac{U_0 L}{\nu}, \quad (50)$$

and  $\Gamma_{cp} = \Gamma L/U_0^2$ . We can also rewrite  $\xi$  as

$$\xi = \Gamma_Y Re L / 2U_0^2. \quad (51)$$

### 6.2. The perturbation analysis

To perform a perturbation analysis for the background flow described by equation (49), we follow the same procedure described in §4.2 and we obtain the corresponding Orr-Sommerfeld and Squire equations similar to equations (24) and (25), given by

$$\left( \frac{\partial}{\partial t} + U \frac{\partial}{\partial y} \right) \nabla^2 u - U'' \frac{\partial u}{\partial y} + \frac{2}{q} \frac{\partial \zeta}{\partial z} - \frac{1}{Re} \nabla^4 u = 0, \quad (52)$$

and

$$\left( \frac{\partial}{\partial t} + U \frac{\partial}{\partial y} \right) \zeta - U' \frac{\partial u}{\partial z} - \frac{2}{q} \frac{\partial u}{\partial z} - \frac{1}{Re} \nabla^2 \zeta = 0, \quad (53)$$

where prime denotes differentiation w.r.to  $x$ . The corresponding no-slip boundary conditions are:  $u = v = w = 0$  at the two boundaries  $x = \pm 1$ , or equivalently  $u = \frac{\partial u}{\partial x} = \zeta = 0$  at  $x = \pm 1$  (see Mukhopadhyay et al. 2005; Ghosh & Mukhopadhyay 2021). We, then, substitute solution forms given by equations (26) and (27), but replacing  $\mathcal{X}$  by  $x$ , in equations (52) and (53), and eventually obtain equation (30) through equations (28) and (29), where  $\mathcal{L}$  and the elements of  $\mathcal{L}$  are given by equations (31) and (32) but replacing  $U_\alpha$ ,  $Re_\alpha$ , and  $\mathcal{D} = \partial/\partial\mathcal{X}$  by  $U$ ,  $Re$ , and  $\mathcal{D} = \partial/\partial x$  respectively.

To have a qualitative idea about the eigenspectra, the analytical exploration based on pure vertical perturbations, shown in §5.2 for plane Poiseuille flow, is of great use. Replacing  $U'_{\alpha Y}$  by  $U'$  in equation (39) for Couette-Poiseuille flow, the growth rate turns out to be

$$\sigma_{CP} = -\frac{\gamma_{CP}}{2} \pm \sqrt{-\frac{4}{q^2} + \frac{4\xi x}{q} + \frac{2}{q}}, \quad (54)$$

where  $\gamma_{CP} = 2k_z^2/Re$ . For the marginal instability, the discriminant in equation (54) becomes zero and hence

$$q = \frac{2}{2\xi x + 1}. \quad (55)$$

If we consider  $\xi = 0$  in the equation (55), we see that the marginal instability occurs at  $q = 2$ . However, for the concerned flow, this condition is relaxed by the presence of  $\xi$ . The constraint on  $q$  can be drawn from the domain

size, i.e.  $|x| \leq 1$ . The restrictions on  $q$  for marginal instability, therefore, are

$$q > \frac{2}{2\xi + 1} \text{ for } x < 1, \quad (56)$$

and

$$q < \frac{2}{1 - 2\xi} \text{ for } x > -1. \quad (57)$$

Similarly, we can obtain the constraint on  $\xi$  too. To have the instability, the discriminant in equation (54) has to follow the condition given by

$$-\frac{4}{q^2} + \frac{4\xi x}{q} + \frac{2}{q} \geq 0 \quad (58)$$

and hence  $\xi x \geq 1/q - 1/2$ . The constraint on  $\xi$ , therefore, is given by

$$\xi > \frac{1}{q} - \frac{1}{2}. \quad (59)$$

For Keplerian flow, i.e.  $q = 1.5$ ,  $\xi > 0.167$ .

FIG. 14 however describes the exact eigenspectra for Couette-Poiseuille flow in the presence of Keplerian rotation ( $q = 1.5$ ) for vertical perturbation with  $k_y = 0$  and  $k_z = 1$  for several  $\xi$  and  $Re$ . As the figure shows, for  $\xi = 0.3$ , the system is unstable, while for  $\xi = 0.15$  and  $0.17$ , the system is stable. This is to remember that the apparent discrepancy between the results based on equation (59) and FIG. 14 is due to the inexact nature of eigenvalue given by equation (54). Equation (54) corresponds to a qualitative description of the vertical perturbation for Couette-Poiseuille flow. While deriving equation (54), we have considered the perturbation to be the function of  $z$  only. However, in reality in order to obtain the eigenvalues (here for vertical perturbation), the perturbation has to be the function of both  $x$  and  $z$ , as indeed was considered in order to obtain eigenspectra given by FIG. 14. This leads to a differential equation of  $x$ , which we solve with no-slip boundary condition to have the eigenspectra. Hence, while equation (54) and the conditions derived from it give the qualitative idea for the eigenspectra, those do not provide the exact information. In FIG. 14, we also notice that for  $\xi = 0.3$ , the system is more unstable for  $Re = 2000$  than  $Re = 1500$ . It is quite easy to understand from equation (54) that keeping other parameters, i.e.,  $q$ ,  $\xi$ , and  $k_z$ , fixed, if we increase  $Re$ ,  $\gamma_{CP}$  decreases, and hence  $\sigma_{CP}$  increases.

FIGs. 15 and 16 describe the eigenspectra for Couette-Poiseuille flow in the presence of rotation with different rotation parameters for vertical and three-dimensional perturbations, respectively. For both cases, we see that as the rotation parameter increases, the system becomes more unstable. If there is no rotation in the system,

it is stable for the parameters considered in these two cases. FIG. 17 depicts an example for the nature of velocity eigenfunction, which is given for the most unstable mode corresponding to Couette-Poiseuille flow with  $Re = 3000$ ,  $k_y = 0.5$ ,  $k_z = 1$ , and  $q = 1.5$ . According to Kersale et al. (2004), these are body modes.

FIGs. 18 and 19 describe the eigenspectra for Couette-Poiseuille flow in the presence of rotation for vertical and three-dimensional perturbations, respectively, for different  $\xi$ . For both cases, we notice that as  $\xi$  increases, the system becomes more unstable. From equation (54), we can qualitatively explain this behavior. The discriminant in equation (54) and hence  $\sigma_{CP}$  increase as  $\xi$  increases for a fixed  $q$ .

FIG. 20 describes the eigenspectra for Couette-Poiseuille flow in the presence of Keplerian rotation for  $k_y = 1$  and various  $k_z$ . We notice that as  $k_z$  increases keeping other parameters fixed, the system becomes more unstable. From equation (32), it is clear that rotation (i.e.  $q$ ) is coupled with  $k_z$  and the shear velocity is coupled with  $k_y$ . As  $k_z$  increases, the effect of rotation in the system, therefore, dominates over the effect of shear. It is now quite evident from the whole discussion that rotation and shear have opposite effects on the stability of the flow. Rotation tries to make the flow more unstable, while shear tries to stabilize it. It is also well-described in FIG. 21. It describes the eigenspectra for Couette-Poiseuille flow in the presence of Keplerian rotation for  $k_z = 1$  and various  $k_y$ . As  $k_y$  increases, the flow becomes more dominated by shear than rotation and hence making the flow more stable.

Interestingly, it is seen from FIGs. 13, 19, 21 that the entire eigenspectrum keeps shifting to the positive  $\sigma_r$  direction with increasing  $k_y$  or  $\xi$ . This can be qualitatively understood in the following analysis. Assuming approximate solutions for equations (52) and (53) be  $u, \zeta \sim \exp(\sigma_{CP3}t + \tilde{\mathbf{k}} \cdot \mathbf{r})$ , where  $\tilde{\mathbf{k}} \equiv (k_x, k_y, k_z)$  and  $\mathbf{r} \equiv (x, y, z)$ , we obtain

$$\sigma_r = \left( U + \frac{U''}{2k^2} \right) k_y \pm f(k_x, k_y, k_z, U', U'', q), \quad (60)$$

where the function  $f(k_x, k_y, k_z, U', U'', q)$  is determined by the natures of background flow, perturbation and rotation,  $\sigma_{CP3} = \sigma_i - i\sigma_r$ , according to our convention of original exact solution given by equation (33) and eigenspectra. Note however that the solution in the  $x$ -direction in principle should not be of the plane wave form as  $U$  is a function of  $x$ , what indeed we do not choose in order to compute eigenspectra. It is easy to check that the magnitude of  $f(k_x, k_y, k_z, U', U'', q)$  is smaller than the first term in the parenthesis in equation (60), and  $\sigma_r$  increases with increasing  $k_y$  for the

background flows and generally the parameters considered here. Therefore, equation (60) confirms that as  $k_y$  increases,  $\sigma_r$  increases, with a shift in the positive  $\sigma_r$  direction, as seen in FIGS. 13 and 21. Similarly, with increasing  $\xi$ , Couette-Poiseuille flow tends to become pure Poiseuille flow and  $\sigma_r \rightarrow (1 - x^2 - 1/\tilde{k}^2)\xi k_y$ . Therefore,  $\xi$  and  $k_y$  play interchangeable roles and, hence, with increasing  $\xi$ ,  $\sigma_r$  increases, as seen in FIG. 19.

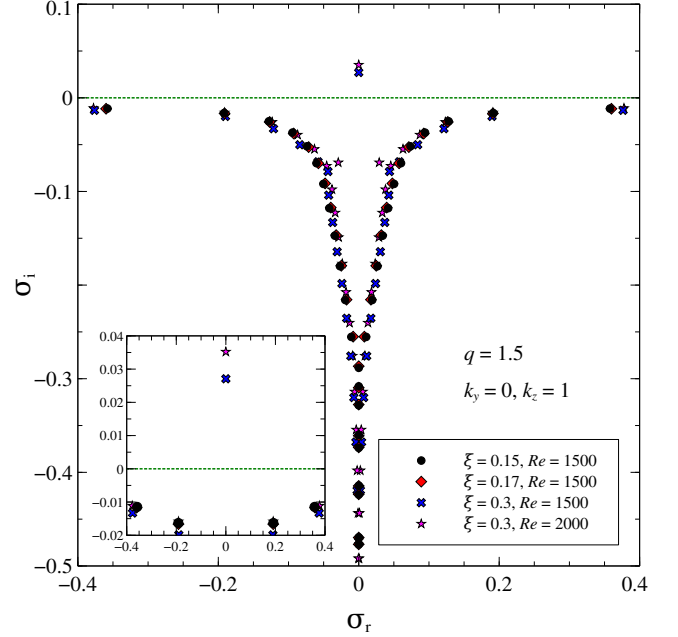
FIG. 22 describes the maximum growth rate ( $\sigma_{i,max}$ ) as a function of  $\xi$  for Couette-Poiseuille flow having a vertical perturbation with  $k_z$  maximizing  $\sigma_i$ . It shows that  $\sigma_{i,max}$  increases monotonically with  $\xi$  for both the  $q$ 's. It also shows that if  $\xi \lesssim 1$ ,  $\sigma_{i,max}$  for  $q = 2$  is larger than that for  $q = 1.5$ . However, the situation reverses for  $\xi > 1$ . This phenomenon can be understood qualitatively from FIG. 23, where we show the variation of  $\sqrt{-4/q^2 + 4\xi x/q + 2/q}$  from equation (54) as a function of  $x$  for several combinations of  $q$  and  $\xi$ . We see that for  $\xi = 0.5$ ,  $\sqrt{-4/q^2 + 4\xi x/q + 2/q}$  is larger for  $q = 2$  than that for  $q = 1.5$ . As a result,  $\sigma_{CP}$  in equation (54) becomes larger for  $q = 2$  than that for  $q = 1.5$ . This explains the behavior of  $\sigma_{i,max}$  for  $\xi \lesssim 1$  in the FIG. 22. Similarly, the explanation of larger  $\sigma_{i,max}$  for  $\xi > 1$  in the FIG. 22 can be extracted from the curves with  $q = 1.5$  and  $q = 2$  at  $\xi = 5.0$ , in the FIG. 23. It is further verified from FIG 22 that below certain  $\xi$ , depending on  $q$ , flow becomes stable with negative  $\sigma_{i,max}$ .

FIG. 24 describes maximum growth rate as a function of  $q$  for Couette-Poiseuille flow with  $\xi = 0.5, 1.0$  and  $Re = 1500$  for vertical perturbation with  $k_z$  maximizing  $\sigma_i$ . It shows that  $\sigma_{i,max}$  increases with increasing  $q$  for  $\xi = 0.5$ . However, for  $\xi = 1$ ,  $\sigma_{i,max}$  increases with increasing  $q$  only up to  $q \sim 1.6$ , subsequently it decreases. This behavior can be qualitatively understood from FIG. 25, where we show the variation of the discriminant in the equation (54) as a function of  $x$  with  $\xi = 1$  and for  $q = 1.0, 1.4, 1.6, 1.8$  and  $2.0$ . It shows that the case of  $q = 1.4$  gives rise to maximum discriminant. However, the maximum discriminants for  $q = 1$  and  $2$  are almost the same and they are the least among all the  $q$ 's. Hence  $\sigma_{CP}$  from equation (54) will be the highest for  $q = 1.4$  and lowest for  $q = 1$  and  $2$ . This qualitative analysis, therefore, indicates that  $\sigma_{i,max}$  is not expected to increase with the increase of  $q$  throughout at any  $\xi$ .

### 6.3. Viable magnitude of force

From the bound on  $\xi$  for Keplerian flow described above, we can have an estimation of the extra force,  $\Gamma_Y$ . From equation (51), we have

$$U_0 = \sqrt{\frac{\Gamma_Y L Re}{2\xi}}. \quad (61)$$



**Figure 14.** Eigenspectra for Couette-Poiseuille flow, described by equation (49), in the presence of Keplerian rotation ( $q = 1.5$ ) for vertical perturbation with  $k_y = 0$  and  $k_z = 1$  for different  $Re$  and  $\xi$ .

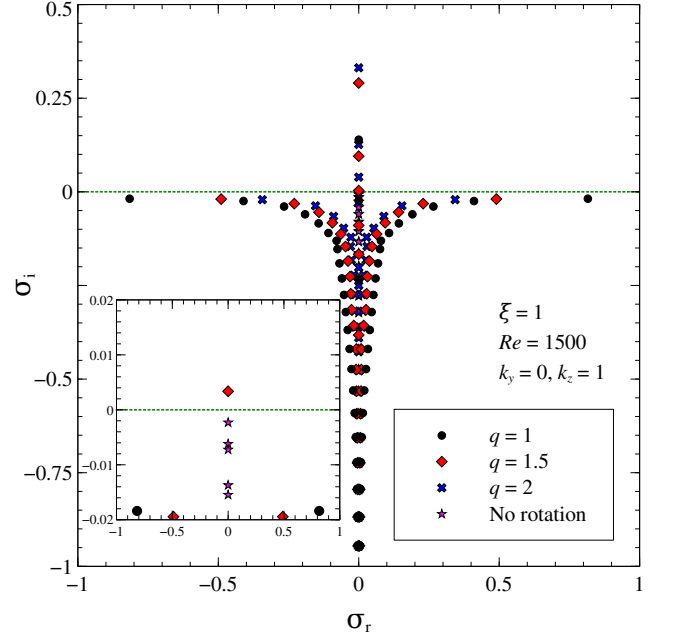


**Figure 15.** Eigenspectra for Couette-Poiseuille flow, described by equation (49), in the presence of rotation for vertical perturbation with  $k_y = 0$  and  $k_z = 1$  for different rotation parameter ( $q$ ),  $Re = 1500$  and  $\xi = 1$ .

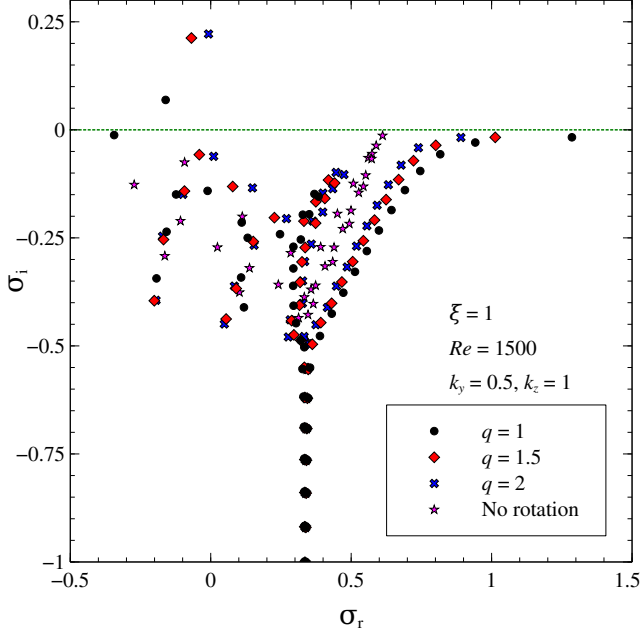


**Figure 16.** Eigenspectra for Couette-Poiseuille flow, described by equation (49), in the presence of rotation for threedimensional perturbation with  $k_y = 0.5$  and  $k_z = 1$  for different rotation parameter ( $q$ ),  $Re = 1500$  and  $\xi = 1$ .

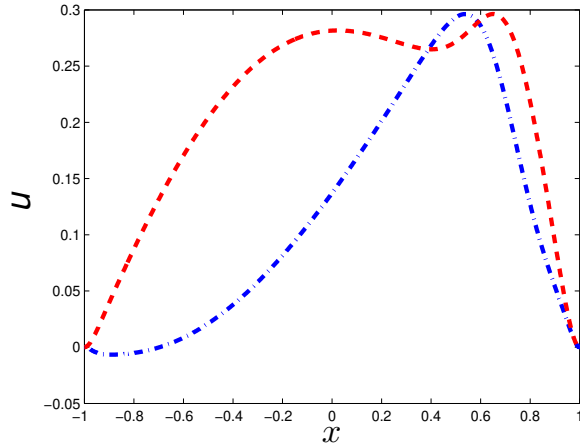


**Figure 17.** Velocity eigenfunction for the most unstable mode corresponding to linearized Couette-Poiseuille flow in the presence of Keplerian rotation ( $q = 1.5$ ) of the box for  $Re = 3000$  with  $k_y = 0.5$  and  $k_z = 1$ . Dot-dashed and dashed lines indicate, respectively, the real and imaginary parts of  $u$ .

The size of the shearing box,  $L$ , is  $0.05R_s$  (Nath & Mukhopadhyay 2015), where  $R_s = 2GM/c^2$  is the Schwarzschild radius for the central black hole of mass  $M$  with  $G$  and  $c$  the gravitational constant and speed of light in free space, respectively. From Mukhopadhyay (2013), we get that for accretion disk,  $Re \gtrsim 10^{14}$ .

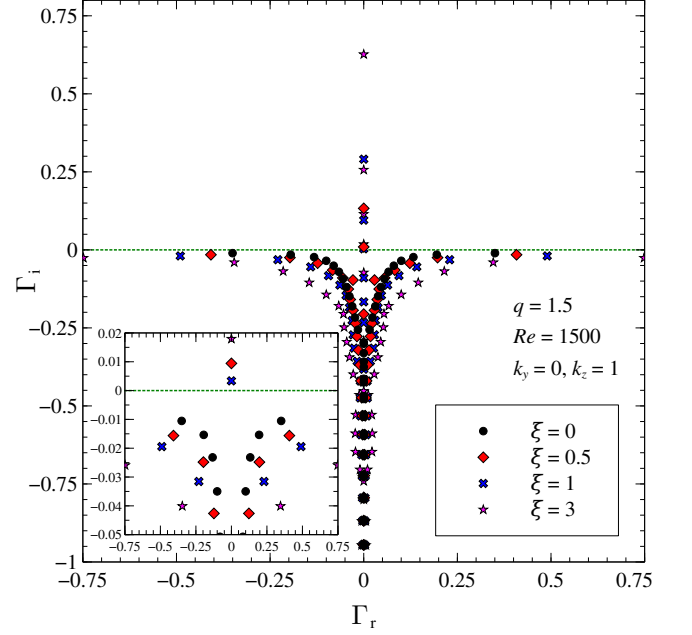


**Figure 18.** Eigenspectra for Couette-Poiseuille flow, described by equation (49), in the presence of Keplerian rotation ( $q = 1.5$ ) for vertical perturbation with  $k_y = 0$  and  $k_z = 1$ ,  $Re = 1500$  and different  $\xi$ .

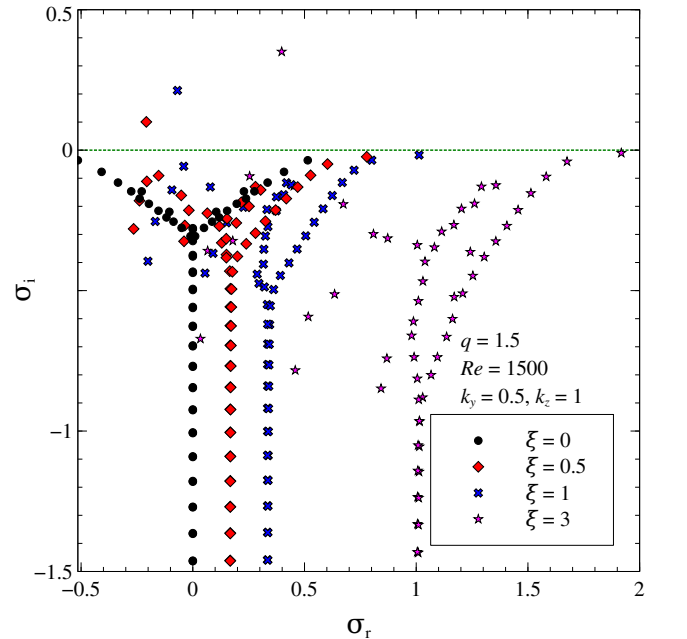


**Figure 19.** Eigenspectra for Couette-Poiseuille flow, described by equation (49), in the presence of Keplerian rotation ( $q = 1.5$ ) for threedimensional perturbation with  $k_y = 0.5$  and  $k_z = 1$ ,  $Re = 1500$  and different  $\xi$ .

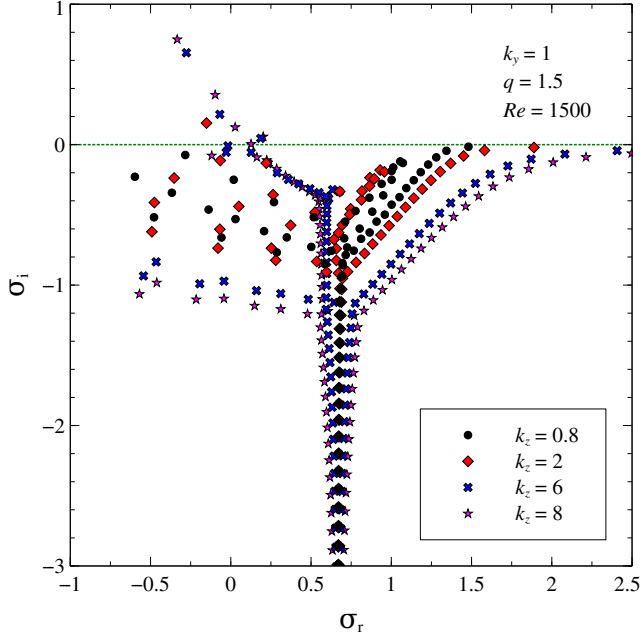


**Figure 20.** Eigenspectra for Couette-Poiseuille flow, described by equation (49), in the presence of Keplerian rotation ( $q = 1.5$ ) for  $k_y = 1$ , different  $k_z$ ,  $Re = 1500$  and  $\xi = 1$ .

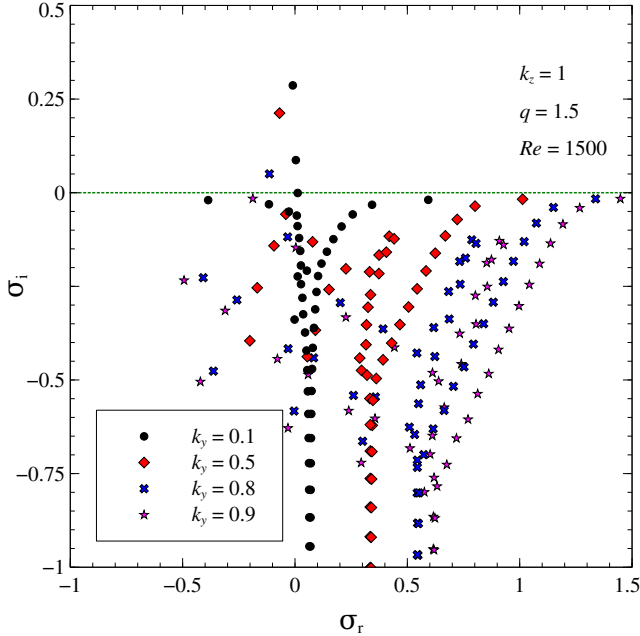


**Figure 21.** Eigenspectra for Couette-Poiseuille flow, described by equation (49), in the presence of Keplerian rotation ( $q = 1.5$ ) for different  $k_y$ ,  $k_z = 1$ ,  $Re = 1500$  and  $\xi = 1$ .

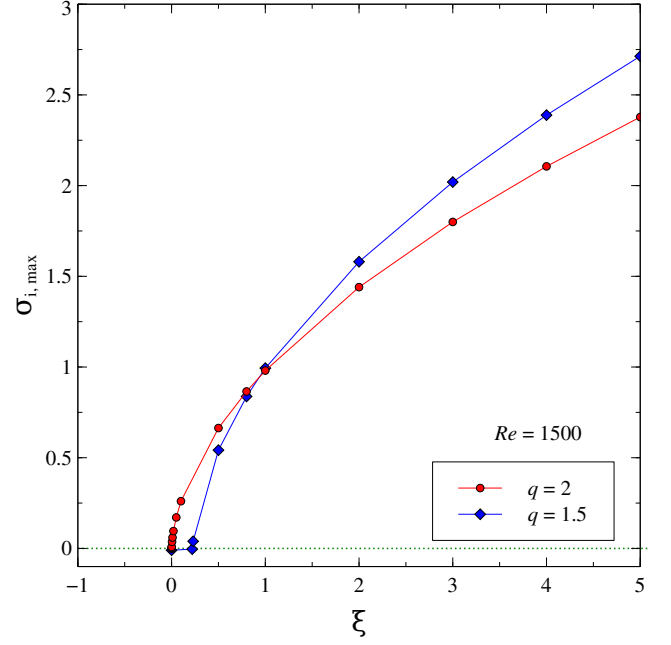


**Figure 22.** Maximum growth rate ( $\sigma_{i, max}$ ) as a function of  $\xi$  for Couette-Poiseuille flow with  $q = 1.5, 2.0$  having vertical perturbation for  $k_z$  maximizing  $\sigma_{i, max}$  and  $Re = 1500$ .

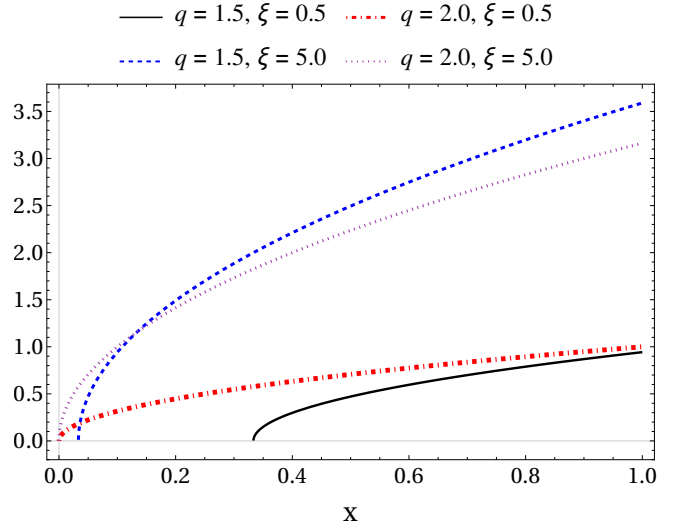


**Figure 23.** Variation of  $\sqrt{-4/q^2 + 4\xi x/q + 2/q}$  from equation (54) as a function of  $x$  for several combinations of  $q$  and  $\xi$ .

Considering all these and the lowest bound on  $\xi$ , i.e.  $\xi = 0.167$  for Keplerian disk, we obtain

$$U_0 = \sqrt{5\bar{m} \bar{n} \Gamma_Y} \times 10^9 \text{ cm/sec} \simeq \sqrt{\bar{m} \bar{n} \Gamma_Y} \frac{c}{10}, \quad (62)$$

where  $Re = \bar{n}10^{14}$ ,  $M = \bar{m}M_\odot$  and  $M_\odot$  is the mass of the Sun. Now at radius  $R$ , the speed would be

$$U_0 = \sqrt{\frac{GM}{R}} = \frac{c}{\sqrt{2\rho}}, \quad (63)$$



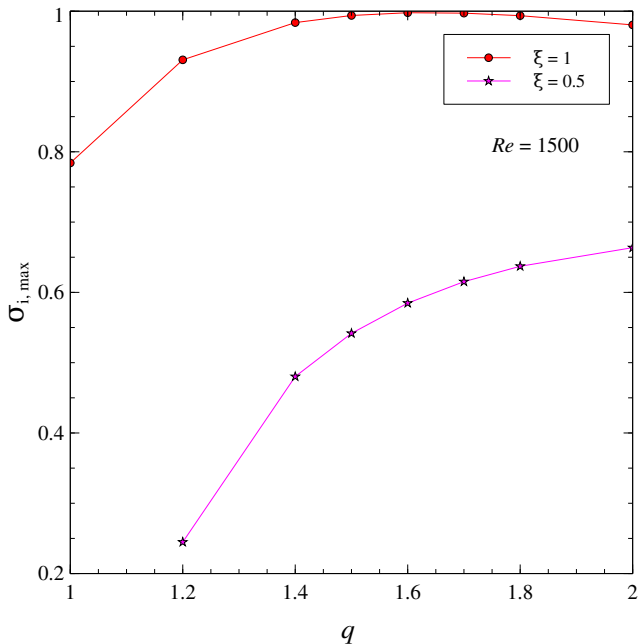


**Figure 24.** Maximum growth rate ( $\sigma_{i,max}$ ) as a function of  $q$  for Couette-Poiseuille flow with  $\xi = 0.5, 1.0$  having vertical perturbation for  $k_z$  maximizing  $\sigma_{i,max}$  and  $Re = 1500$ .

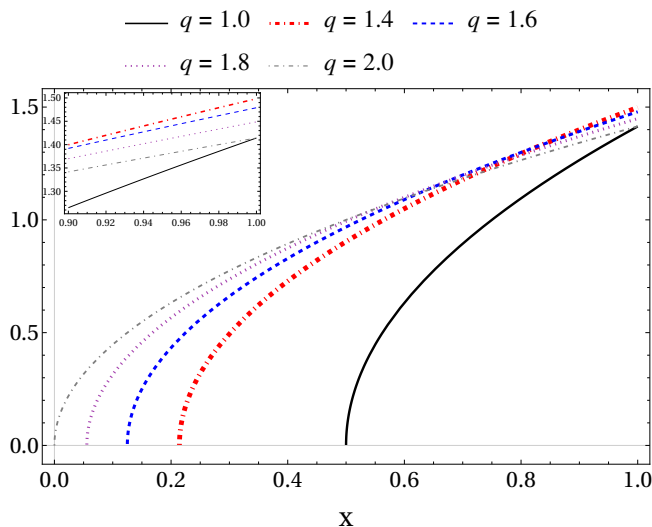


**Figure 25.** Variation of  $\sqrt{-4/q^2 + 4\xi x/q + 2/q}$  from equation (54) as a function of  $x$  for  $\xi = 1$  and for several  $q$ 's.

where,  $R = \rho R_s$ . If the fluid is at  $100R_s$ , then  $U_0 = c/10\sqrt{2}$ . From equations (62) and (63), we obtain  $\Gamma_Y = 0.5/\bar{m} \bar{n}$  cm/sec<sup>2</sup>. This confirms that the extra force indeed is very small for the accretion disk around an astrophysical black hole whose  $Re$  is huge. For example, a supermassive black hole of mass  $10^7 M_\odot$  having accretion disk with  $Re = 10^{22}$  leads to  $\Gamma_Y = 5 \times 10^{-16}$  cm/sec<sup>2</sup> which is too small compared to the acceleration due to the gravity of the black hole at that position. This con-

**Table 1.** Critical values of Reynolds number ( $Re_{\alpha,critic}$ ) and critical values of  $k_z$  ( $k_{z,critic}$ ) for three different rotation parameter  $q$  for plane Poiseuille flow in the presence of rotation for vertical perturbation, i.e.  $k_y = 0$ .

$q$	$Re_{\alpha,critic}$	$k_{z,critic}$
2.0	137.2969	4.066
1.8	174.84	4.5762
1.5	327.58	6.1

firms that indeed a tiny  $\Gamma_Y$ , i.e., a very small effect of external force would make the flow unstable.

## 7. ACCURACY OF NUMERICS

Throughout the work, we have used the finite difference method to obtain the eigenspectra. We particularly have used the second order central difference method. Equation (34) is an eigenvalue equation, which is function  $x$ . To solve it numerically, we discretize the domain which ranges from  $x = x_0 = -1$  to  $x = x_f = 1$ . In our calculation, we have divided the domain in  $(N + 1)$  segments, where the width of the each segment is defined as

$$h = \frac{x_f - x_0}{N + 1}. \quad (64)$$

For all the eigenspectra presented in this work,  $N = 499$ . Therefore, the dimension of  $\mathcal{L}$  in equation (34) after using finite difference method is  $2N \times 2N$ . To check the accuracy and the convergence of the eigenvalues for the chosen matrix dimension, we show the variation of Error =  $\sigma_{i,max}(N) - \sigma_{i,max}(N = 1099)$  as a function of  $N$  in FIG. 26 for a typical set of parameters. It confirms that chosen  $N = 499$  leads to the optimum numerical values of  $\sigma_i$  which hardly changes with further increasing  $N$ . Infact, variation of  $\sigma_{i,max}$  for  $199 \leq N \leq 1099$  is not more than  $\sim 10^{-4}$ .

However, to check the accuracy of the eigenspectra, particularly the most unstable modes as these are the most important feature of this work, we have also verified the result of finite difference method with those obtained using Chebfun (Driscoll et al. 2014). FIG. 27 demonstrates the eigenspectra for Couette-Poiseuille flow for a given set of parameters. It confirms that both the eigenspectra match quite well with each other, hence the accuracy of our results.

## 8. DISCUSSION

In the previous sections, we have observed that stability of rotating Poiseuille flow and Couette-Poiseuille flow greatly depends on  $q$ , and also on the nature of perturbation. To make this statement more concrete, we show in FIG. 28 the eigenspectra of plane Poiseuille flow

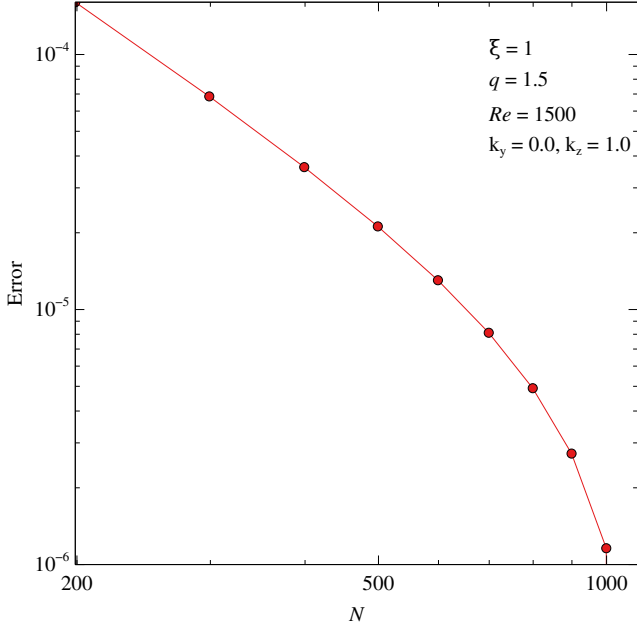


**Figure 26.** Error as a function of  $N$  for Couette-Poiseuille flow with  $\xi = 1$ ,  $q = 1.5$ ,  $Re = 1500$ ,  $k_y = 0$  and  $k_z = 1.0$ .

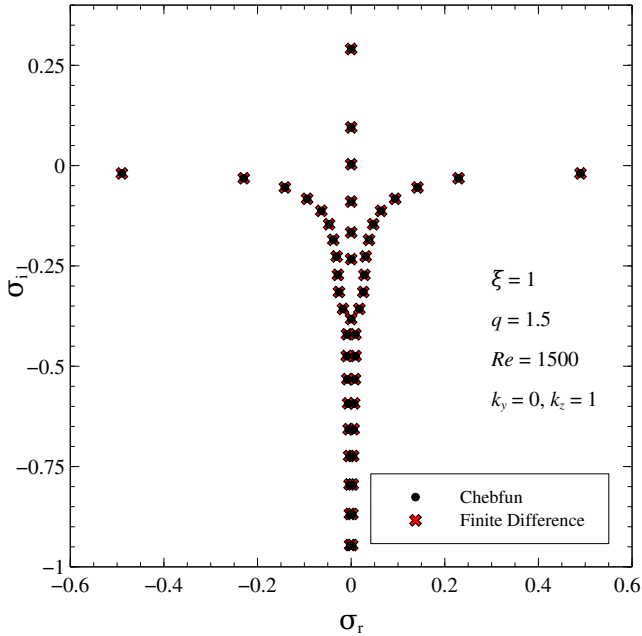


**Figure 27.** Eigenspectra for Couette-Poiseuille flow with  $\xi = 1$  in the presence of Keplerian rotation for  $Re = 1500$ ,  $k_y = 0$  and  $k_z = 1$ , obtained using Chebfun and finite difference methods.

in the presence and absence of rotation for three-dimensional perturbation with  $k_y = k_z = 1$ . Here, we notice that Poiseuille flow is stable even for  $Re_\alpha = 10000$  with  $k_y = k_z = 1$ , when rotational effect has not been taken into account. On the contrary, when rotation is there,

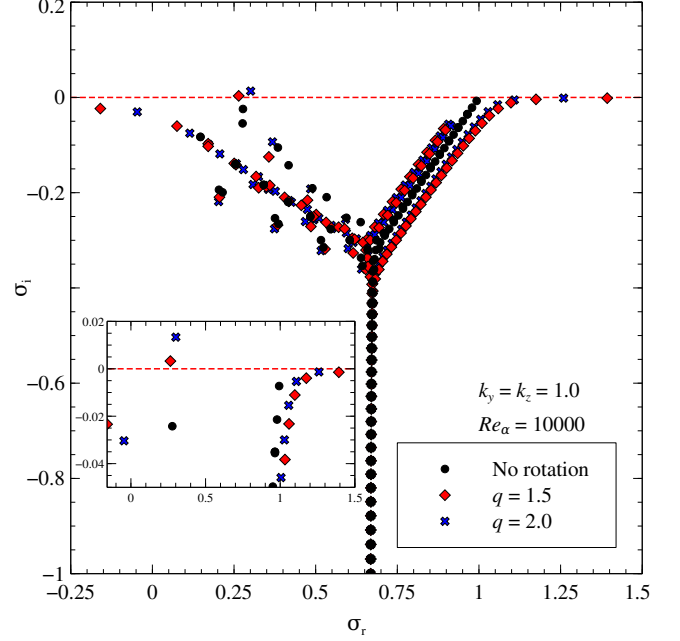


**Figure 28.** Eigenspectra of linearized Poiseuille flow in the presence of rotation for three-dimensional perturbation with  $k_y = k_z = 1$  for three different  $q$  and  $Re_\alpha = 10000$ .

the flow becomes unstable, and as  $q$  increases, the maximum growth rate increases for the same set of other parameters. We, therefore, argue that rotation makes plane Poiseuille flow unstable. On the other hand, rotation has an opposite effect on plane Couette flow. It is clear from equation (39) by substituting  $U_{\alpha Y} = -\mathcal{X}$  and hence  $U'_{\alpha Y} = -1$ . Equation (39) then becomes

$$\sigma = -\frac{\gamma}{2} \pm \frac{\sqrt{2}}{q} \sqrt{q-2}, \quad (65)$$

and hence

$$\sigma = -\frac{\gamma}{2} \pm \frac{i}{\Omega q} \kappa, \quad (66)$$

where  $\kappa$  is the epicyclic frequency, given by  $\kappa = \Omega \sqrt{2(2-q)}$ . Now for  $q < 2$ ,  $\kappa$  is always a positive real number and, hence, plane Couette flow with rotational effect is always stable as long as  $q < 2$ . On the other hand, equation (40) shows that even if  $q < 2$ , plane Poiseuille flow with rotation becomes unstable in a particular domain of flow depending on  $q$ .

In §5.3, we have argued that as  $q$  increases for a fixed  $Re_\alpha$ , the maximum growth rates increases. This statement quite matches with the literature, i.e. [Lezius & Johnston 1976](#) (its figure 2), [Alfredsson & Persson 1989](#). However, those authors considered ‘ $Ro$ ’ as the rotation parameter and it is inverse of  $q$ . Apart from that, the background flow considered by them is  $6(\mathcal{X} - \mathcal{X}^2)$ . This is the reason behind obtaining different critical  $Re$  and wavevector in the present work than those by [Lezius](#)

& Johnston (1976) and Finlay (1990) (see their table 1). While they obtained critical  $Re \sim 89$  and critical wavevector  $\sim 5$ , we have obtained them as 137.2969 and 4.066 respectively for the vertical perturbation and  $q = 2$ , e.g., as provided in TABLE. 1 which enlists the critical  $Re$  ( $Re_{\alpha,critic}$ ) and the critical wavevector ( $k_{z,critic}$ ) for different rotation parameters. We notice that  $Re_{\alpha,critic}$  increases as  $q$  decreases, as expected from the whole discussion.

Note importantly that the inclusion of rotation does not invalidate the Squire theorem which states that a flow that is unstable in three dimensions, will be unstable in two dimensions at a lower  $Re$ . It is obvious from FIGs. 13 and 21. As  $k_y$  is nonzero and increases further, keeping other parameters fixed, we see that the growth rate most unstable mode or least stable mode decreases.

## 9. CONCLUSION

In the presence of extra force, plane Couette flow behaves more like plane Poiseuille flow. However, depending on the strength of force and the boundary conditions, it may almost behave like plane Couette flow, or the deviation from plane Couette flow may be small. Nevertheless, when this flow is studied in the presence of Coriolis effect, it becomes unstable under threedimensional perturbations as well as pure vertical perturbations. In fact, rotational effect makes the flow more unstable and, hence, turbulence inside the underlying shearing box is inevitable.

In the literature before this work, when the hydrodynamic instability of the Keplerian accretion flow has been studied in the local region, the flow has been approximated to plane Couette flow with rotation embedded in it. However, recent works (Nath & Mukhopadhyay 2016; Ghosh & Mukhopadhyay 2020; Razdoburdin 2020) suggest that the presence of an extra force (random or constant) is inevitable in such a flow, at least the effect of external force worth exploring. We, therefore, have argued here that the background flow of a local Keplerian accretion disk will deviate from plane Couette flow. We, in fact, have considered here such deviated background flow modifying to plane Poiseuille flow. This modification depends on the strength of force and the boundary conditions. Controlling these two factors,

plane Couette flow and also its nature can be revived. We know that plane Poiseuille flow is unstable beyond the respective critical values of certain parameters for planer perturbation. We, therefore, can argue that the local Keplerian flow becomes unstable due to the presence of an extra force.

However, the effect of Coriolis force, which is inevitable for shearing box in the Keplerian disk, makes the problem more interesting. We know that rotation stabilizes the linear shear flow. However, for plane Poiseuille flow, it has opposite effects. In the presence of rotation, plane Poiseuille flow becomes unstable at a  $Re$  which is about two orders of magnitude less than that required for the instability without rotation. We have shown here that as the rotation parameter  $q$  increases, the flow becomes more unstable (or at least less stable) for a particular set of parameters. The important point here is that the presence of an extra force modifies the local Keplerian flow from linear shear to nonlinear shear and the Coriolis effect makes it unstable for a very small  $Re$ . We have also argued that even the presence of a tiny force, that could lead to required amount of deviation from the linear shear, makes it unstable even in the presence of rotation. Once the flow becomes unstable, eventually it is expected to become nonlinear and turbulent. It, therefore, helps us to understand the sub-critical transition to turbulence in hydrodynamic accretion flow and other laboratory flows where external forcing, however tiny be, is unavoidable.

## ACKNOWLEDGMENT

S.G. acknowledges DST India for INSPIRE fellowship. We are thankful to Laurette S. Tuckerman of the Centre national de la recherche scientifique and Dwight Barkley of the University of Warwick for the discussion that influenced us to initiate this work and further discussion for better presentation. We also thank Tushar Mondal and Sudeb Ranjan Datta of Indian Institute of Science for their comments and suggestions. We are thankful to the referee for insightful suggestions and comments that help present the work in a better way. This work is partly supported by a fund of Department of Science and Technology (DST-SERB) with research Grant No. DSTO/PPH/BMP/1946 (EMR/2017/001226).

## APPENDIX

### A. THE DERIVATION OF THE BACKGROUND FLOW IN THE LOCAL REGION OF THE KEPLERIAN ACCRETION DISK

Let us consider a fluid element inside the box at the point  $P$ . With respect to  $C$ , the flow is along the  $\phi$  direction. Inside the box, however, the flow will be along the  $y$ -direction only. Now let us assume the velocity at  $P$  with respect

to the box be  $V_Y$ . Nevertheless, the velocity at the same point with respect to  $C$  would be  $R\Omega_0 + V_Y$ . Had there been no shearing box, the velocity of the fluid at the point  $P$  will be  $\Omega R$  with respect to  $C$ . Hence,

$$\begin{aligned}
 R\Omega_0 + V_Y &= \Omega R \Rightarrow V_Y = R(\Omega - \Omega_0) \\
 &= R(\Omega(R_0 + X) - \Omega(R_0)), [R - R_0 = X \ll R_0, R] \\
 &= R \left[ \Omega(R_0) + X \left( \frac{d\Omega}{dR} \right)_{R_0} + \dots - \Omega(R_0) \right] \\
 &\cong RX \left( \frac{d\Omega}{dR} \right)_{R_0} \\
 &= -q\Omega_0 X \frac{R}{R_0} \\
 &= -q\Omega_0 X \left( 1 + \frac{X}{R_0} \right) \\
 &\cong -q\Omega_0 X.
 \end{aligned} \tag{A1}$$

## REFERENCES

- Afshordi, N., Mukhopadhyay, B., & Narayan, R. 2005, *ApJ*, 629, 373, doi: [10.1086/431418](https://doi.org/10.1086/431418)
- Alfredsson, P. H., & Persson, H. 1989, *Journal of Fluid Mechanics*, 202, 543, doi: [10.1017/S002211208900128X](https://doi.org/10.1017/S002211208900128X)
- Avila, M. 2012, *Physical Review Letters*, 108, 124501, doi: [10.1103/PhysRevLett.108.124501](https://doi.org/10.1103/PhysRevLett.108.124501)
- Bai, X.-N. 2013, *ApJ*, 772, 96, doi: [10.1088/0004-637X/772/2/96](https://doi.org/10.1088/0004-637X/772/2/96)
- . 2017, *ApJ*, 845, 75, doi: [10.3847/1538-4357/aa7dda](https://doi.org/10.3847/1538-4357/aa7dda)
- Balakumar, P. 1997, *Theoretical and Computational Fluid Dynamics*, 9, 103, doi: [10.1007/s001620050035](https://doi.org/10.1007/s001620050035)
- Balbus, S. A. 2003, *ARA&A*, 41, 555, doi: [10.1146/annurev.astro.41.081401.155207](https://doi.org/10.1146/annurev.astro.41.081401.155207)
- Balbus, S. A., & Hawley, J. F. 1991, *ApJ*, 376, 214, doi: [10.1086/170270](https://doi.org/10.1086/170270)
- Balbus, S. A., Hawley, J. F., & Stone, J. M. 1996, *ApJ*, 467, 76, doi: [10.1086/177585](https://doi.org/10.1086/177585)
- Bhatia, T. S., & Mukhopadhyay, B. 2016, Exploring nonnormality in magnetohydrodynamic rotating shear flows: application to astrophysical accretion disks. <https://arxiv.org/abs/1609.01841>
- Cantwell, C. D., Barkley, D., & Blackburn, H. M. 2010, *Physics of Fluids*, 22, 034101, doi: [10.1063/1.3313931](https://doi.org/10.1063/1.3313931)
- Chagelishvili, G. D., Zahn, J. P., Tevzadze, A. G., & Lominadze, J. G. 2003, *A&A*, 402, 401, doi: [10.1051/0004-6361:20030269](https://doi.org/10.1051/0004-6361:20030269)
- Chandrasekhar, S. 1960, *Proceedings of the National Academy of Science*, 46, 253, doi: [10.1073/pnas.46.2.253](https://doi.org/10.1073/pnas.46.2.253)
- Cowley, S. J., & Smith, F. T. 1985, *Journal of Fluid Mechanics*, 156, 83, doi: [10.1017/S0022112085002002](https://doi.org/10.1017/S0022112085002002)
- Das, U., Begelman, M. C., & Lesur, G. 2018, *Mon. Not. Roy. Astron. Soc.*, 473, 2791, doi: [10.1093/mnras/stx2518](https://doi.org/10.1093/mnras/stx2518)
- Dauchot, O., & Daviaud, F. 1995, *Physics of Fluids*, 7, 335, doi: [10.1063/1.868631](https://doi.org/10.1063/1.868631)
- Driscoll, T. A., Hale, N., & Trefethen, L. N. 2014. <http://www.chebfun.org>
- Dubrulle, B., Dauchot, O., Daviaud, F., et al. 2005a, *Physics of Fluids*, 17, 095103, doi: [10.1063/1.2008999](https://doi.org/10.1063/1.2008999)
- Dubrulle, B., Marié, L., Normand, C., et al. 2005b, *A&A*, 429, 1, doi: [10.1051/0004-6361:200400065](https://doi.org/10.1051/0004-6361:200400065)
- Finlay, W. H. 1990, *Journal of Fluid Mechanics*, 215, 209, doi: [10.1017/S0022112090002622](https://doi.org/10.1017/S0022112090002622)
- Frank, J., King, A., & Raine, D. J. 2002, *Accretion Power in Astrophysics: Third Edition*, 398
- Gammie, C. F., & Menou, K. 1998, *The Astrophysical Journal*, 492, L75, doi: [10.1086/311091](https://doi.org/10.1086/311091)
- Ghosh, S., & Mukhopadhyay, B. 2020, *MNRAS*, doi: [10.1093/mnras/staa1780](https://doi.org/10.1093/mnras/staa1780)
- Ghosh, S., & Mukhopadhyay, B. 2021, *Phys. Rev. Fluids*, 6, 013903, doi: [10.1103/PhysRevFluids.6.013903](https://doi.org/10.1103/PhysRevFluids.6.013903)
- Hains, F. D. 1967, *Physics of Fluids*, 10, 2079, doi: [10.1063/1.1762411](https://doi.org/10.1063/1.1762411)
- Hawley, J. F., Balbus, S. A., & Winters, W. F. 1999, *The Astrophysical Journal*, 518, 394, doi: [10.1086/307282](https://doi.org/10.1086/307282)
- Hawley, J. F., Gammie, C. F., & Balbus, S. A. 1995, *ApJ*, 440, 742, doi: [10.1086/175311](https://doi.org/10.1086/175311)
- Ioannou, P. J., & Kakouris, A. 2001, *ApJ*, 550, 931, doi: [10.1086/319791](https://doi.org/10.1086/319791)
- Kersale, E., Hughes, D. W., Ogilvie, G. I., Tobias, S. M., & Weiss, N. O. 2004, *The Astrophysical Journal*, 602, 892, doi: [10.1086/381194](https://doi.org/10.1086/381194)

- Kim, W.-T., & Ostriker, E. C. 2000, *ApJ*, 540, 372, doi: [10.1086/309293](https://doi.org/10.1086/309293)
- Klahr, H. H., & Bodenheimer, P. 2003, *ApJ*, 582, 869, doi: [10.1086/344743](https://doi.org/10.1086/344743)
- Klotz, L., Lemoult, G., Frontczak, I., Tuckerman, L. S., & Wesfreid, J. E. 2017, *Physical Review Fluids*, 2, 043904, doi: [10.1103/PhysRevFluids.2.043904](https://doi.org/10.1103/PhysRevFluids.2.043904)
- Lesur, G., & Longaretti, P.-Y. 2005, *A&A*, 444, 25, doi: [10.1051/0004-6361:20053683](https://doi.org/10.1051/0004-6361:20053683)
- Lezius, D. K., & Johnston, J. P. 1976, *Journal of Fluid Mechanics*, 77, 153, doi: [10.1017/S0022112076001171](https://doi.org/10.1017/S0022112076001171)
- Lynden-Bell, D., & Pringle, J. E. 1974, *Monthly Notices of the Royal Astronomical Society*, 168, 603, doi: [10.1093/mnras/168.3.603](https://doi.org/10.1093/mnras/168.3.603)
- Mahajan, S. M., & Krishan, V. 2008, *ApJ*, 682, 602, doi: [10.1086/589321](https://doi.org/10.1086/589321)
- Menou, K. 2000, *Science*, 288, 2022, doi: [10.1126/science.288.5473.2022](https://doi.org/10.1126/science.288.5473.2022)
- Menou, K., & Quataert, E. 2001, *ApJ*, 552, 204, doi: [10.1086/320466](https://doi.org/10.1086/320466)
- Mukhopadhyay, B. 2013, *Physics Letters B*, 721, 151, doi: [10.1016/j.physletb.2013.02.056](https://doi.org/10.1016/j.physletb.2013.02.056)
- Mukhopadhyay, B., Afshordi, N., & Narayan, R. 2005, *ApJ*, 629, 383, doi: [10.1086/431419](https://doi.org/10.1086/431419)
- Mukhopadhyay, B., & Chattopadhyay, A. K. 2013, *Journal of Physics A Mathematical General*, 46, 035501, doi: [10.1088/1751-8113/46/3/035501](https://doi.org/10.1088/1751-8113/46/3/035501)
- Mukhopadhyay, B., Mathew, R., & Raha, S. 2011, *New Journal of Physics*, 13, 023029, doi: [10.1088/1367-2630/13/2/023029](https://doi.org/10.1088/1367-2630/13/2/023029)
- Nath, S. K., & Mukhopadhyay, B. 2015, *PhRvE*, 92, 023005, doi: [10.1103/PhysRevE.92.023005](https://doi.org/10.1103/PhysRevE.92.023005)
- . 2016, *ApJ*, 830, 86, doi: [10.3847/0004-637X/830/2/86](https://doi.org/10.3847/0004-637X/830/2/86)
- Ogilvie, G. I., & Pringle, J. E. 1996, *MNRAS*, 279, 152, doi: [10.1093/mnras/279.1.152](https://doi.org/10.1093/mnras/279.1.152)
- Orszag, S. A. 1971, *Journal of Fluid Mechanics*, 50, 689, doi: [10.1017/S0022112071002842](https://doi.org/10.1017/S0022112071002842)
- Paoletti, M. S., van Gils, D. P. M., Dubrulle, B., et al. 2012, *A&A*, 547, A64, doi: [10.1051/0004-6361/201118511](https://doi.org/10.1051/0004-6361/201118511)
- Papaloizou, J. C. B., & Pringle, J. E. 1984, *MNRAS*, 208, 721, doi: [10.1093/mnras/208.4.721](https://doi.org/10.1093/mnras/208.4.721)
- Pessah, M. E., & Psaltis, D. 2005, *ApJ*, 628, 879, doi: [10.1086/430940](https://doi.org/10.1086/430940)
- Razdoburdin, D. N. 2020, *Perturbations dynamics in Keplerian flow under external stochastic forcing*. <https://arxiv.org/abs/2001.03912>
- Richard, D., & Zahn, J.-P. 1999, *Astron. Astrophys.*, 347, 734. <https://arxiv.org/abs/astro-ph/9903374>
- Rüdiger, G., & Zhang, Y. 2001, *A&A*, 378, 302, doi: [10.1051/0004-6361:20011214](https://doi.org/10.1051/0004-6361:20011214)
- Savenkov, I. V. 2010, *Computational Mathematics and Mathematical Physics*, 50, 1399, doi: [10.1134/S0965542510080105](https://doi.org/10.1134/S0965542510080105)
- Shakura, N. I., & Sunyaev, R. A. 1973, *Astron. Astrophys.*, 24, 337
- Tevzadze, A. G., Chagelishvili, G. D., Zahn, J. P., Chanishvili, R. G., & Lominadze, J. G. 2003, *A&A*, 407, 779, doi: [10.1051/0004-6361:20030867](https://doi.org/10.1051/0004-6361:20030867)
- Velikhov, E. 1959, *Zhur. Eksptl'. i Teoret. Fiz.*, Vol: 36
- Xiong, X., & Tao, J. 2020, *Physics of Fluids*, 32, 094104, doi: [10.1063/5.0015737](https://doi.org/10.1063/5.0015737)
- Yecko, P. A. 2004, *A&A*, 425, 385, doi: [10.1051/0004-6361:20041273](https://doi.org/10.1051/0004-6361:20041273)